

REPORT DOCUMENTATION PAGE			Form Approved OMB NO. 0704-0188		
<p>The public reporting burden for this collection of information is estimated to average 1 hour per response, including the time for reviewing instructions, searching existing data sources, gathering and maintaining the data needed, and completing and reviewing the collection of information. Send comments regarding this burden estimate or any other aspect of this collection of information, including suggestions for reducing this burden, to Washington Headquarters Services, Directorate for Information Operations and Reports, 1215 Jefferson Davis Highway, Suite 1204, Arlington VA, 22202-4302. Respondents should be aware that notwithstanding any other provision of law, no person shall be subject to any penalty for failing to comply with a collection of information if it does not display a currently valid OMB control number.</p> <p>PLEASE DO NOT RETURN YOUR FORM TO THE ABOVE ADDRESS.</p>					
1. REPORT DATE (DD-MM-YYYY) 21-10-2014		2. REPORT TYPE MS Thesis		3. DATES COVERED (From - To) -	
4. TITLE AND SUBTITLE Study of the surface morphology of thermally annealed copper foils and various transfer methods for graphene			5a. CONTRACT NUMBER W911NF-10-1-0450		
			5b. GRANT NUMBER		
			5c. PROGRAM ELEMENT NUMBER 611102		
6. AUTHORS O. Sarajlic			5d. PROJECT NUMBER		
			5e. TASK NUMBER		
			5f. WORK UNIT NUMBER		
7. PERFORMING ORGANIZATION NAMES AND ADDRESSES Georgia State University Research Foundati PO Box 3999  Atlanta, GA 30302 -3999			8. PERFORMING ORGANIZATION REPORT NUMBER		
9. SPONSORING/MONITORING AGENCY NAME(S) AND ADDRESS (ES) U.S. Army Research Office P.O. Box 12211 Research Triangle Park, NC 27709-2211			10. SPONSOR/MONITOR'S ACRONYM(S) ARO		
			11. SPONSOR/MONITOR'S REPORT NUMBER(S) 58093-EL.25		
12. DISTRIBUTION AVAILABILITY STATEMENT Approved for public release; distribution is unlimited.					
13. SUPPLEMENTARY NOTES The views, opinions and/or findings contained in this report are those of the author(s) and should not contrued as an official Department of the Army position, policy or decision, unless so designated by other documentation.					
14. ABSTRACT The surface morphology of thermally annealed copper foils utilized for graphene growth by chemical vapor deposition (CVD) has been studied by Optical microscopy, Scanning Electron Microscopy (SEM), and Scanning Tunneling Microscopy (STM) as a function of heat treatment. This study reports on the surface roughness and relative grain size before and after thermal annealing. The main results are that (a) the graphene covered foil exhibits reduced surface roughness, and (b) the graphene film preserves an imprint of the Cu grain structure. In the second part of the work, the transfer of CVD graphene is experimentally investigated using Poly(method					
15. SUBJECT TERMS CVD graphene, transfer methods for graphene, thermally annealed copper foils, chemical vapor depostion,					
16. SECURITY CLASSIFICATION OF:			17. LIMITATION OF ABSTRACT UU	15. NUMBER OF PAGES	19a. NAME OF RESPONSIBLE PERSON Ramesh Mani
a. REPORT UU	b. ABSTRACT UU	c. THIS PAGE UU			19b. TELEPHONE NUMBER 404-413-6007

## **Report Title**

Study of the surface morphology of thermally annealed copper foils and various transfer methods for graphene

### **ABSTRACT**

The surface morphology of thermally annealed copper foils utilized for graphene growth by chemical vapor deposition (CVD) has been studied by Optical microscopy, Scanning Electron Microscopy (SEM), and Scanning Tunneling Microscopy (STM) as a function of heat treatment. This study reports on the surface roughness and relative grain size before and after thermal annealing. The main results are that (a) the graphene covered foil exhibits reduced surface roughness, and (b) the graphene film preserves an imprint of the Cu grain structure. In the second part of the work, the transfer of CVD graphene is experimentally investigated using Poly(methyl methacrylate) (PMMA), Polycarbonate (PC), and Polystyrene (PS). Noticeable improvement to surface cleanliness as well as electrical properties of graphene is observed after the ethanol treatment. Finally, Raman characterization showed apparent blue-shifts of the G and 2D bands suggesting that the graphene is heavily doped after the ethanol treatment.

STUDY OF THE SURFACE MORPHOLOGY OF THERMALLY ANNEALED COPPER FOILS  
AND VARIOUS TRANSFER METHODS FOR GRAPHENE

by

OLESYA SARAJLIC

Under the Direction of Ramesh Mani

ABSTRACT

The surface morphology of thermally annealed copper foils utilized for graphene growth by chemical vapor deposition (CVD) has been studied by Optical microscopy, Scanning Electron Microscopy (SEM), and Scanning Tunneling Microscopy (STM) as a function of heat treatment. This study reports on the surface roughness and relative grain size before and after thermal annealing. The main results are that (a) the graphene covered foil exhibits reduced surface roughness, and (b) the graphene film preserves an imprint of the Cu grain structure. In the second part of the work, the transfer of CVD graphene is experimentally investigated using Poly(methyl methacrylate) (PMMA), Polycarbonate (PC), and Polystyrene (PS). Noticeable improvement to surface cleanness as well as electrical properties of graphene is observed after the ethanol treatment. Finally, Raman characterization showed apparent blue-shifts of the G and 2D bands suggesting that the graphene is heavily doped after the ethanol treatment.

INDEX WORDS: Graphene, Chemical Vapor Deposition, Average roughness, Surface height variations, Graphene transfer, Thermoplastic polymers (PMMA, PC, PS), Ethanol

STUDY OF THE SURFACE MORPHOLOGY OF THERMALLY ANNEALED COPPER FOILS  
AND VARIOUS TRANSFER METHODS FOR GRAPHENE

by

OLESYA SARAJLIC

A Thesis Submitted in Partial Fulfillment of the Requirements for the Degree of

Master of Science

in the College of Arts and Sciences

Georgia State University

2013



STUDY OF THE SURFACE MORPHOLOGY OF THERMALLY ANNEALED COPPER FOILS  
AND VARIOUS TRANSFER METHODS FOR GRAPHENE

by

OLESYA SARAJLIC

Committee Chair: Ramesh Mani

Committee: Vadim Apalkov  
Douglas Gies  
Zhigang Jiang  
Unil Perera

Electronic Version Approved:

Office of Graduate Studies

College of Arts and Sciences

Georgia State University

December 2013

## ACKNOWLEDGEMENTS

I express my deep gratitude and appreciation to my thesis supervisor, Dr. Ramesh G. Mani for his influential guidance and support throughout this research. I have been extremely fortunate to have an advisor who gave me the freedom to explore on my own. His interesting ideas and constructive counsels have motivated me toward production of this thesis. I am also indebted to the members of the Nanoscience Laboratory, Tianyu Ye, Han-Chun Liu, and Zhuo Wang, with whom I have interacted during the course of my graduate studies. I wish to thank them for their generous support in the laboratory facility during the experiments and data accumulation stages. I would also like to thank my committee members, Vadim Apalkov, Douglas Gies, Zhigang Jiang, and Unil Perera for their instructive support and valued counsels.

Most importantly, I would like to express my sincere gratitude to all of my family members, especially to my mother and father for their constant support and inspiration throughout this research work toward Master Degree. And most of all, I would like to thank my loving, supportive, encouraging, and patient husband, Semir, whose faithful support throughout this graduate program is greatly appreciated. The support and care of my immediate family helped me overcome obstacles and stay focused on my graduate study.

I would like to thank Rachana Singh and John Hankinson at Georgia Institute of Technology for their assistance with Raman measurements. I gratefully acknowledge the funding agencies that made my graduate work possible. The work for this thesis has been supported by the DOE-BES, MSE Division under DE-SC0001762, and the additional support was provided by the ARO under W911NF-07-01-0158.

## TABLE OF CONTENTS

<b>ACKNOWLEDGEMENTS .....</b>	<b>v</b>
<b>LIST OF TABLES .....</b>	<b>vi</b>
<b>LIST OF FIGURES.....</b>	<b>ix</b>
<b>1 INTRODUCTION .....</b>	<b>1</b>
1.1 Carbon allotropes.....	1
1.2 Methods of graphene synthesis .....	2
<b>2 THEORETICAL BACKGROUND .....</b>	<b>6</b>
2.1 Atomic structure of graphene .....	6
2.2 Electronic properties .....	7
2.3 Applications .....	8
<b>3 GRAPHENE SYNTHESIS, TRANSFER, AND FABRICATION .....</b>	<b>9</b>
3.1 Exfoliated graphene .....	9
3.2 Epitaxial graphene on Silicon Carbide .....	10
3.3 Chemical Vapor Deposition .....	11
3.3.1 Transfer methods .....	12
<b>4 EXPERIMENTAL CHARACTERIZATIONS AND RESULTS .....</b>	<b>14</b>
4.1 Copper foil annealing process .....	14
4.2 Optical characterizations .....	15
4.2.1 Optical microscopy.....	15
4.2.2 Scanning Electron Microscopy.....	18
4.2.3 Scanning Tunneling Microscopy.....	21
4.3 Transfer process .....	23
4.4 Raman Spectrum .....	24



<b>5</b>	<b>EFFECTS ON COPPER SURFACE MORPHOLOGY: DISCUSSION .....</b>	<b>26</b>
<b>6</b>	<b>POLYMER SUPPORT METHODS.....</b>	<b>28</b>
6.1	Effect of Ethanol Treatment.....	29
6.2	Raman Characterizations of Ethanol Treated Graphene.....	31
6.3	Electrical Measurements as a Function of Polymer Support .....	33
6.4	Graphene Surface Tears.....	35
<b>7</b>	<b>SUMMARY AND FUTURE WORK .....</b>	<b>37</b>
	<b>REFERENCES .....</b>	<b>39</b>
	<b>APPENDICES .....</b>	<b>44</b>
	<b>Appendix A: List of Abbreviations .....</b>	<b>44</b>
	<b>Appendix B: Methods .....</b>	<b>45</b>
	<i>Appendix B.1: Graphene Growth in Chapter 4.....</i>	<i>45</i>
	<i>Appendix B.2: Graphene Growth in Chapter 6 .....</i>	<i>45</i>
	<i>Appendix B.3: Graphene Transfer in Chapter 4.....</i>	<i>46</i>
	<i>Appendix B.4: Graphene Transfer in Chapter 6.....</i>	<i>46</i>
	<i>Appendix B.5: Sample Fabrication Technique in Chapter 6.....</i>	<i>46</i>
	<i>Appendix B.6: Optical Technology Classifications in Chapter 4.....</i>	<i>47</i>
	<i>Appendix B.7: Optical Technology Classifications in Chapter 6.....</i>	<i>47</i>

**LIST OF TABLES**

Table 1.1 Latest reports of sample size and room temperature charge carrier mobility of mono-layer graphene synthesized by different methods.....	3
Table 4.1 Description of the protocols applied to the unetched bare foil (BF) and the etched foil (EF) of copper .....	15
Table 6.1 Molecular characteristics of thermoplastic polymers (PMMA, PC, and PS) and ethanol (ethyl alcohol). Molecular formula defines corresponding molecular structure. The geometry of PC and PS shows the existence of benzene rings that are attached to the carbon atom on the backbone of their chemical structures unlike the one of PMMA. Molecular characteristics of ethanol demonstrate the presence of hydroxyl group ( $-C_2H_5$ ) that is able to dissolve many ionic and polar compounds and ethyl group ( $-OH$ ) that attracts non-polar substances.....	28

## LIST OF FIGURES

Figure 1.1 Multi-dimensional $sp^2$ -bonded carbon: (a) 0D buckyball structure, (b) 1D single-walled carbon nanotubes, (c) 2D graphene, (d) 3D graphite .....	1
Figure 2.1 (a) AFM topography of graphene deposited on $SiO_2$ substrate. (b) Large area STM image of mechanically exfoliated graphene sheet on $SiO_2$ substrate. (c) STM images of atomic-scale resolution of mechanically exfoliated graphene film on $SiO_2$ wafer .....	6
Figure 2.2 Schematic of the band structure of graphene, where two in-equivalent points, K and K', at the vertex of the Brillouin zone display no energy gap between two sublattices.....	7
Figure 2.3 Potential graphene applications in industry and research .....	8
Figure 3.1 Exfoliated graphene: (a) process of mechanical exfoliation of graphene from bulk graphite using scotch tape, (b) single layer graphene transferred on $SiO_2$ wafer .....	9
Figure 3.2 Epitaxial graphene on Silicon Carbide: (a) schematics of epitaxial graphene on silicon carbide showing buffer layer and Si- and C-termination, (b) atomic force microscope (AFM) image of graphene/ $SiC$ terraces.....	10
Figure 3.3 Graphene synthesized by CVD. (a) CVD growth process, where hydrogen atoms support the reaction between methane and catalytic substrate during which process carbon atoms are chemically adsorbed on the metal surface. (b) SEM image of CVD graphene on copper substrate with copper striations and grain boundaries are clearly visible. (c) CVD graphene transferred onto $SiO_2$ substrate after copper has been chemically removed .....	12
Figure 3.4 Schematic illustration of wet transfer process of CVD grown graphene on copper foil onto $SiO_2$ substrate .....	13
Figure 3.5 (a) Optical micrograph of CVD graphene on $SiO_2$ substrate, (b) Raman spectroscopy of the transferred graphene on $SiO_2$ substrate in image (a) illustrating the presence of single-layer (brown curve), bilayer (blue curve), and few-layer graphene (black curve) with identified D, G, and 2D peaks ..	13
Figure 4.1 (a) Schematics of the CVD system. (b) Photo of the experimental set-up of CVD growth furnace .....	14
Figure 4.2 Optical images of 25 $\mu m$ Cu foil at 400 $\times$ magnification. The label at the top right of the images indicates the protocol to which the specimen was subjected, see also Table 4.1. BF indicates bare foil, EF indicates etched foil. (a) This panel shows that bare foil includes striations resulting from rolling copper at high pressure. (b) Bare foil subjected to a $Fe(NO_3)_3$ etch produces a nonuniform surface with micrometer sized pores.....	16
Figure 4.3 Optical images of 25 $\mu m$ Cu foil at 400 $\times$ magnification. The label at the top right of the images indicates the protocol to which the specimen was subjected, see also Table 4.1. BF indicates bare foil, EF indicates etched foil, $H_2N_2$ indicates heat treatment in forming gas at 1025 $^{\circ}C$ for 30 min. (a) Bare Cu foil heat treated in $H_2N_2$ at 1025 $^{\circ}C$ for 30 min displays a 250 $\mu m$ wide copper grain along with traces of stri-	

ations that are less pronounced after thermal treatment. (b) Etched foil treated in  $\text{H}_2\text{N}_2$  at 1025 °C for 30 min displays few hundreds micrometer wide grains with surface scars ..... 17

Figure 4.4 Optical images of 25  $\mu\text{m}$  Cu foil at 400 $\times$  magnification. The label at the top right of the images indicates the protocol to which the specimen was subjected, see also Table 4.1. BF indicates bare foil, EF indicates etched foil,  $\text{H}_2\text{N}_2$  indicates heat treatment in forming gas at 1025 °C for 30 min, and  $\text{H}_2\text{N}_2:\text{CH}_4$  indicates heat treatment in forming gas and methane at 1025 °C for 30 min. (a) Bare foil thermally exposed to  $\text{H}_2\text{N}_2:\text{CH}_4$  shows graphene on top of copper grains. Here, vertical striations are still visible in the underlying copper foil. (b) Etched foil heat treated under  $\text{H}_2\text{N}_2:\text{CH}_4$  at 1025 °C for 30 min indicates indistinct Cu grains covered with a single layer of graphene. Also visible are micrometer sized pits and dents ..... 17

Figure 4.5 Optical images of 25  $\mu\text{m}$  Cu foil at 400 $\times$  magnification. The label at the top right of the images indicates the protocol to which the specimen was subjected, see also Table 4.1. BF indicates bare foil, EF indicates etched foil,  $\text{H}_2\text{N}_2$  indicates heat treatment in forming gas at 1025 °C for 30 min, and  $\text{H}_2\text{N}_2:\text{CH}_4$  indicates heat treatment in forming gas and methane at 1025 °C for 30 min. (a) Bare foil subjected to heat treatment under  $\text{H}_2\text{N}_2$  at 1025 °C for 30 min followed by  $\text{H}_2\text{N}_2:\text{CH}_4$  at 1025 °C for 30 min displays single layer graphene film overlying Cu grains that are a few hundreds micrometers wide. Inset: A partially peeled Cu foil (scale bar is 500  $\mu\text{m}$ ) that lost the crust layer. (b) Etched foil subjected to heat treatment under  $\text{H}_2\text{N}_2$  at 1025 °C for 30 min followed by  $\text{H}_2\text{N}_2:\text{CH}_4$  at 1025 °C for 30 min shows less surface nonuniformity and includes monolayer graphene ..... 18

Figure 4.6 SEM images of 25  $\mu\text{m}$  Cu foil. The label at the top right of the images indicates the protocol to which the specimen was subjected, see also Table 4.1. BF indicates bare foil, EF indicates etched foil. (a) Striations resulting from rolling copper at high pressure are still visible in the SEM image. Also visible are microscopic dents/fractures in the foil surface. (b) Bare foil subjected to a  $\text{Fe}(\text{NO}_3)_3$  etch produces a nonuniform surface with etch quarries encrusted onto the surface ..... 19

Figure 4.7 SEM images of 25  $\mu\text{m}$  Cu foil. The label at the top right of the images indicates the protocol to which the specimen was subjected, see also Table 4.1. BF indicates bare foil, EF indicates etched foil,  $\text{H}_2\text{N}_2$  indicates heat treatment in forming gas at 1025 °C for 30 min. (a) Heat treated bare Cu foil displays an approximately 50  $\mu\text{m}$  wide grain. (b) Etched foil heat treated under  $\text{H}_2\text{N}_2$  also displays an approximately 50  $\mu\text{m}$  wide grain ..... 19

Figure 4.8 SEM images of 25  $\mu\text{m}$  Cu foil. The label at the top right of the images indicates the protocol to which the specimen was subjected, see also Table 4.1. BF indicates bare foil, EF indicates etched foil,  $\text{H}_2\text{N}_2$  indicates heat treatment in forming gas at 1025 °C for 30 min, and  $\text{H}_2\text{N}_2:\text{CH}_4$  indicates heat treatment in forming gas and methane at 1025 °C for 30 min. (a) Well pronounced 20–30  $\mu\text{m}$  wide flower-shaped structures are observed on the surface of copper once the Cu foil has been treated with  $\text{H}_2\text{N}_2:\text{CH}_4$ . Vertically running striations are still evident on the left. These flower structures suggest graphene grains that have not yet coalesced into a uniform and continuous sheet of graphene. (b) This panel shows graphene domains, with multiple wrinkles within them, that are on the verge of coalescing together to cover the underlying metallic substrate ..... 20

Figure 4.9 SEM images of 25  $\mu\text{m}$  Cu foil. The label at the top right of the images indicates the protocol to which the specimen was subjected, see also Table 4.1. BF indicates bare foil, EF indicates etched foil,  $\text{H}_2\text{N}_2$  indicates heat treatment in forming gas at 1025 °C for 30 min, and  $\text{H}_2\text{N}_2:\text{CH}_4$  indicates heat treatment in forming gas and methane at 1025 °C for 30 min. (a) This figure shows the Cu surface nearly fully

covered with graphene. (b) The image shows the graphene layer overlying micrometer sized pits in the etched Cu foil ..... 20

Figure 4.10 (a) STM image of bare Cu foil that shows a granular surface with average grain diameter of about 20 nm. (b) This figure shows a 10 nm height variation in the bare foil over a 0.2  $\mu\text{m}$  interval in the domain  $0 \leq x \leq 0.3 \mu\text{m}$ , with  $R_a = 0.25 \text{ nm}$  over the line trace..... 22

Figure 4.11 (a) STM image of unetched Cu foil exposed to  $\text{H}_2\text{N}_2$ . The grains appear to be flattened. (b) Cross-sectional profile showing 3 nm height variation with average surface roughness of 0.18 nm in the  $\text{H}_2\text{N}_2$  annealed foil..... 23

Figure 4.12 (a) STM image of unetched Cu foil heat treated in  $\text{H}_2\text{N}_2:\text{CH}_4$  for 30 min at 1025  $^\circ\text{C}$ . This protocol produces a monolayer graphene sheet that covers the underlying catalytic substrate. Inset: Atomic resolution image of graphene on copper (scale bar is 2 nm). (b) Cross-sectional profile showing 10 nm height variations with average surface roughness of 0.08 nm in  $\text{H}_2\text{N}_2:\text{CH}_4$  treated foil. .... 23

Figure 4.13 Schematic diagram of graphene transfer procedure onto silicon dioxide substrate ..... 24

Figure 4.14 (a) Cu foil with graphene (see Figures 4.4a and 4.8a) was etched in  $\text{Fe}(\text{NO}_3)_3$  and transferred onto  $\text{SiO}_2$  wafer using a PMMA transfer technique. Here, traces of Cu grain boundaries appear imprinted on the graphene layer. (b) Raman spectrum of the graphene film obtained with 532 nm laser excitation ..... 25

Figure 6.1 SEM images of CVD graphene on  $\text{SiO}_2$  substrate. (a) Graphene transferred via PMMA support showing visible wrinkles (blue errors) and graphene grains of about 2  $\mu\text{m}$  each side of a hexagon. Scattered residuals of the polymer are clearly visible on the surface of the film. (b) Graphene transferred by PMMA, etched in acetone to remove PMMA, and then submerged to the ethanol bath. No noticeable wrinkles are observed, but the graphene grains of about 2  $\mu\text{m}$  in length per side are present. (c) Graphene transferred by PC aid showing excess of polymer residuals on the surface. Graphene grains are still visible through the layer of unetched remnants of PC. (d) Graphene transferred by PC, etched in dichloromethane to remove PC, and then submerged to the ethanol bath. Ethanol treatment has evidently improved the cleanness of graphene film from polymer deposits. Graphene grains are still reproducible and clearly visible. (e) Graphene transferred by PS support showing visible adlayers (red errors) and graphene grains of about 2  $\mu\text{m}$  each side of a hexagon. No visible residue of PS is observed. (f) Graphene transferred by PS, etched in toluene to remove thin layer of polymer support, and then submerged to the ethanol. Ethanol treatment does not have an observable effect on the appearance of the surface cleanness. Visible wrinkles (blue errors), adlayers (red errors), and graphene grains are observed on the surface of transferred graphene film..... 30

Figure 6.2 (a) Raman spectra of CVD graphene on  $\text{SiO}_2$  substrate (using 532 nm wavelength laser) transferred by PMMA (bottom blue curve), PMMA then ethanol treatment (bottom red curve), PC (middle blue curve), PC then ethanol treatment (middle red curve), PS (top blue curve), and PS then ethanol treatment (top red curve). Raman spectrography shows consistent blue-shift of the curves of graphene that were treated by ethanol, regardless of the polymer support used during the transfer. (b) Raman characteristics of CVD graphene on  $\text{SiO}_2$  substrate transferred by PMMA, PC, and PC polymer support materials in addition to those exposed to the ethanol bath, indicated as EG PMMA, EG PC, and EG PS. (c) G-band and 2D-band peak positions as a function of transferred polymer that are extracted from corre-

sponding Raman spectra (a). Both peaks trend to exhibit a blue-shift after the graphene films were exposed to ethanol..... 32

Figure 6.3 Mobility of CVD graphene samples as a function of transfer polymer. The bar chart compares the ethanol treatment impact on the electrical characteristics of transferred graphene (G) by PMMA, PC, and PS. Ethanol treated graphene (EG) samples have a tendency to exhibit higher mobility regardless of the polymer aid that is used for transfer..... 36

Figure 6.4 SEM images of CVD graphene on  $\text{SiO}_2$  substrate that have been treated with ethanol. (a) Large scale graphene film transferred via PMMA support showing no visible breaks or tears of graphene membrane. (b) Graphene transferred by PC aid showing larger area tears (yellow errors) and no visible fractures or laceration of graphene film. (c) Graphene transferred by PS support showing visible small but frequent tears (yellow errors) along with partial laceration (turquoise errors) of the membrane going across the chain of slits..... 36

## 1 INTRODUCTION<sup>1</sup>

Graphene is a novel two-dimensional (2D) material with remarkable electrical and mechanical properties with many potential applications [1-4]. It is a one-atom thick sheet of  $sp^2$ -bonded carbon atoms arranged in a honeycomb lattice. The discovery of this material follows in the footsteps of the discovery of other carbon allotropes such as zero-dimensional (0D) buckyballs, and one-dimensional (1D) multi- and single-walled carbon nanotubes.

### 1.1 Carbon Allotropes

Ordered carbon structures include the multi-dimensional carbon-nanomaterials as seen in Figure 1.1. Graphite is a 3D material that is obtained by stacking of graphene (2D material) layers that are being held together by van der Waals interactions. If a single or multi- sheet of graphene is rolled up on itself, the outcome of the procedure would represent a 1D single-walled or multi-walled carbon nanotube. A graphene sheet rolled up into a sphere would represent a 0D a buckyball.

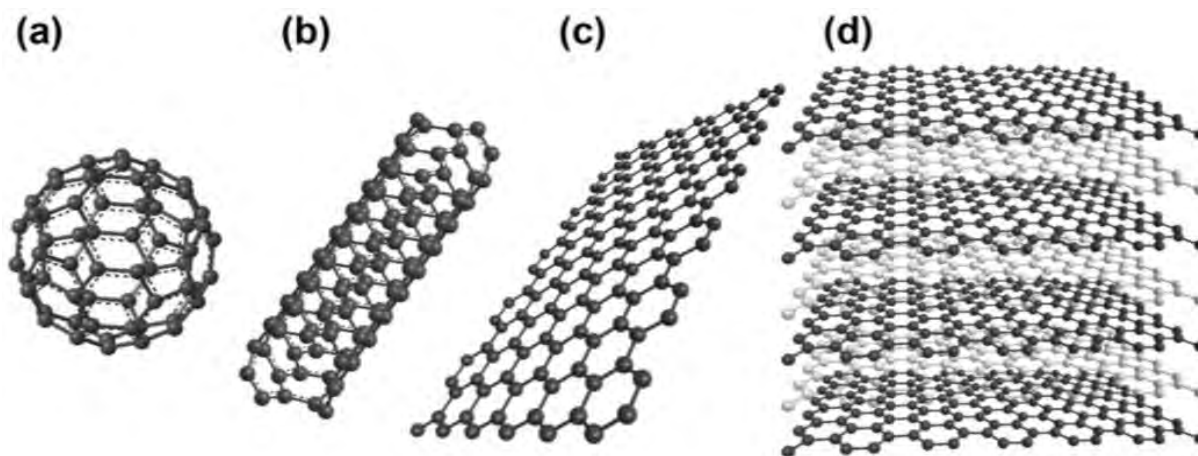


Figure 1.1 Multi-dimensional  $sp^2$ -bonded carbon: (a) 0D buckyball structure, (b) 1D single-walled carbon nanotubes, (c) 2D graphene, (d) 3D graphite [14].

<sup>1</sup> Some contents in this chapter were published in Chemistry of Materials: Sarajlic, O. I.; Mani, R. G. "Mesoscale Scanning Electron and Tunneling Microscopy Study of the Surface Morphology of Thermally Annealed Copper Foils for Graphene Growth". Chem. Mater. 2013, 25, 1643–1648.

## 1.2 Methods of graphene synthesis

The growth of high quality graphene has become a topic of interest as graphene is an exceptional two-dimensional (2D) material with extraordinary electrical and mechanical properties [4,7,8,15-17]. There have been utilized several methods of graphene growth including the epitaxial growth on SiC, method of exfoliation of graphite, and chemical vapor deposition (CVD) [4,7,8,15,16]. Graphene fabricated by the micromechanical cleavage of graphite has been widely utilized to demonstrate the basic properties of graphene [4,15]. Although this method provides high quality graphene, it is not suitable for large scale graphene production, because the graphene flakes are small and scattered randomly on the substrate. Epitaxial growth of graphene on silicon carbide (SiC) gives high quality graphene with high carrier mobility ( $\sim 10,000 \text{ cm}^2/\text{Vs}$ ) [16,18-20]. Epitaxial graphene is produced by the thermal decomposition of SiC at high temperatures between  $1200^\circ\text{C}$  and  $2000^\circ\text{C}$ . Here, the number of graphene layers depends upon the growth temperature, growth time, and other details of the growth process [19,20]. Further, graphene grown on SiC is hard to transfer onto other substrates. The CVD approach utilizes thin foils of copper or nickel as catalysts to decompose organic compounds at a high temperature. The resulting carbon atoms turn into adatoms on the catalyst surface, and subsequently become bonded together in a hexagonal lattice, to form a large area graphene film

Table 1.1 Latest reports of sample size and room temperature charge carrier mobility of mono-layer graphene synthesized by different methods.

Production Method	Maximum Sample Size (mm)	RT Charge Carrier Mobility ( $\text{cm}^2/\text{Vs}$ )	Corresponding References
Mechanical exfoliation	$\sim 1$	$>100,000$	4, 28
Epitaxial growth on SiC	$\sim 100$	$>10,000$	19,20
Chemical Vapor Deposition	$\sim 1000$	$>16,000$	29 - 31



[7]. Table 1.1 summarizes the maximal reported sample size and room temperature (RT) charge carrier mobility of graphene obtained by different methods.

Among the described methods, growth of graphene by CVD on catalytic copper surface [5-9] is particularly attractive for a large-area synthesis. The key feature of copper (Cu) is the reduced solubility of carbon on Cu that facilitates a large-area and uniform growth of a single layer graphene [5,6,21-27]. Unlike other

substrates, Cu allows for the growth of graphene through the adsorption process, where the attractive interaction between C adatoms on the flat Cu surface is believed to promote island formation and fast growth [27,32]. Previous works demonstrated that CVD growth, even on polycrystalline Cu films, results in good quality and large size single layer graphene [4,33-35]. Here, during the CVD growth, carbon atoms follow the surface structure and bind more readily at the Cu grain boundary, which promotes grain boundary defects [27,32,36]. Advances such as electropolishing of the substrate, the two-step CVD process, and the pulsed CVD method serve to eliminate the Cu grain boundaries [29,37,38]. Since the mechanical strength of CVD graphene membrane [39-41] depends on the reduction of defects, these methods help to realize higher quality graphene [37]. Similarly, chemical pre-treatment and/or pre-annealing of the foil can be important growth parameters. It is known that chemical pre-treatment of the foil [42] before CVD growth helps to remove native oxides from the Cu foil, and the high temperature pre-anneal reconstructs the Cu foil surface and promotes grain growth [29]. Yet, further improvements to the CVD graphene quality seem to call for a better understanding of the evolution of the surface of the Cu foil under heat treatment, and the identification of factors such as surface roughness, grain size, and the nature of the grain boundaries that influence graphene quality [4,43].

The goal of the study, which will be discussed in detail in Chapter 4, is to trace and understand the evolution of the surface morphology of the commercially available 25  $\mu\text{m}$  thick copper foil through chemical etching and high-temperature anneal in order to develop better conditions for graphene

growth by CVD. For this purpose, a standard set of protocols were followed in the treatment of the copper foils. We examine changes in the copper morphology as a function of chemical and thermal treatments using various imaging technologies such as optical microscopy, scanning electron microscopy (SEM), and scanning tunneling microscopy (STM). Following from the fact that carbon binds more readily at the Cu grain boundary during CVD growth, optical micrography reveals imprinted macroscopic structures of copper onto the subsequently grown graphene layer once it has been transferred onto the SiO<sub>2</sub> substrate [9].

Graphene grown by CVD on the copper foil needs to be removed from the foil and transferred onto a target substrate before it can electronic device fabrication. The Poly(methyl methacrylate) (PMMA) method is commonly used as an aid to isolate CVD graphene films from the copper substrate. Even though PMMA support is regarded as the standard method of transfer for graphene, previous studies suggest that the acetone treatment and/or thermal annealing in forming gas generally fail to completely remove the residue of PMMA from the surface of graphene [12,44,45]. Furthermore, it was shown that the high temperature anneal induces structural disorders due to the presence of charged impurities between the graphene and SiO<sub>2</sub> substrate [46-48] or potential cracks and tears for supported and free-standing graphene [12,44].

As alternative polymers to PMMA for CVD graphene transfer, polycarbonate (PC) and polystyrene (PS) exhibit excellent mechanical properties which are due to their strength and flexibility. All these polymers are transparent and rigid. However, unlike PMMA, PC is stronger and usable over a greater temperature range without cracking or breaking, and PS has good insulating properties along with low water absorption [49]. It is well known that graphene's properties are greatly affected by numerous factors such as polymer residues from the transfer support [50], charged impurities in the substrate, and absorbents on the graphene surface [51,52]. Thus, there remain issues to be overcome even after the graphene transfer stage in the device fabrication process.

Chapter 6 evaluates the PC and PS polymers for their applicability as alternative materials to PMMA for the graphene transfer. It also discusses an alternative way to decompose the residuals of the polymer from the graphene surface. The ideal polymer support is expected to help to realize a clean and tear-free transfer of graphene onto  $\text{SiO}_2$  substrate, while at the same time being completely dissolved in a readily available standard solvent without leaving the residue on the surface of graphene film. PMMA, PC, and PS have been tested in this study as all of them are thermoplastic polymers with a common ability to act as a thin layer of transport material. The main difference between the suggested thermoplastic polymers, PMMA, PC, and PS, is the chemical composition of the molecule. Unlike PMMA, PC and PS contain benzene rings that are attached to the carbon atom on the backbone of their chemical structures. Having a benzene ring attached to one side of the chain will greatly affect the stiffness of the material [53].

In an attempt to improve the electrical properties of graphene, the Hall bar devices that were exposed to PMMA, PC, and PS support polymers were treated in ethanol. Plastics are commonly absorbent to organic chemicals the effects of which include dissolution and/or recrystallization [54]. Thus, ethanol treatment may potentially rearrange the polymer residue where the hydroxyl functional group is able to dissolve many ionic and polar compounds while the ethyl group attracts non-polar substances [55]. A visible improvement of the surface morphology along with enhanced electrical properties of graphene has been observed after the chemical treatment with ethanol.

Raman spectroscopy is utilized to analyze the behavior of G and 2D peaks as a function of thermoplastic polymer and ethanol treatment. The results suggest that graphene that was exposed to the ethanol makes both G and 2D bands to shift to higher wavenumbers. In addition, ethanol treatment has a tendency to dope graphene more p-type.

## 2 THEORETICAL BACKGROUND

The exceptional electronic and optical properties of graphene have attracted enormous attention and interest. The basic properties and advantages of graphene have been discovered by Andre Geim and Konstantin Novoselov in their innovative research on 2D material graphene [1], for which they received the Nobel Prize in Physics in 2010.

### 2.1 Atomic structure of graphene

Graphene results from the arrangement of carbon atoms in a 2D honeycomb structure. The honeycomb structure may be viewed as a lattice with a basis, with two carbon atoms per unit cell. STM can be used to achieve atomic-scale resolution of graphene. The mesoscale structure of graphene can be determined by atomic force microscope (AFM) as seen from Figure 2.1a. Figure 2.1 shows the atomic structure and nanoscale morphology of single layer of graphene on  $\text{SiO}_2$  substrate. Figures 2.1b – 2.1c show a large-area along with the atomically resolved STM images of graphene film.

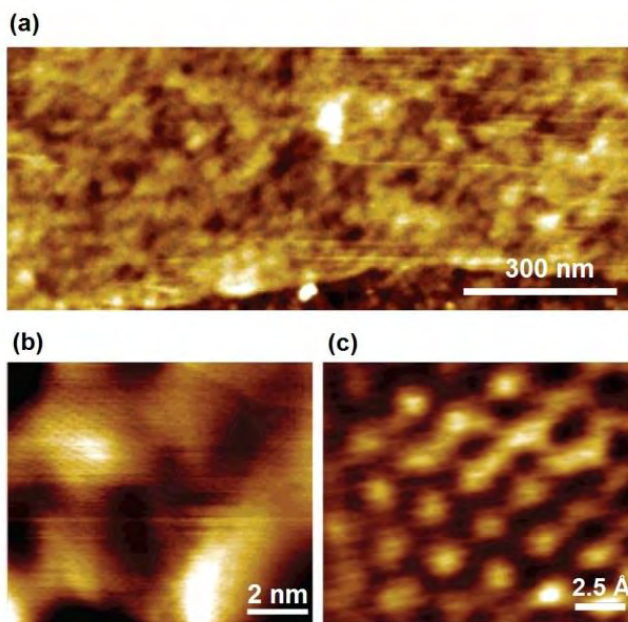


Figure 2.1 (a) AFM topography of graphene deposited on  $\text{SiO}_2$  substrate. (b) Large area STM image of mechanically exfoliated graphene sheet on  $\text{SiO}_2$  substrate. (c) STM images of atomic-scale resolution of mechanically exfoliated graphene film on  $\text{SiO}_2$  wafer [50].

## 2.2 Electronic properties

The electronic structure of graphene strongly influences graphene-based electronics and devices [58]. Monolayer graphene is a zero-gap 2D semiconductor. Graphene's band structure shows a hexagonal symmetry due to the honeycomb lattice of graphene. Since there are two atoms per unit cell in graphene, the band structure shows two in-equivalent points, K and K', see Figure 2.2 [59]. At K and K' Valley points, the energy versus momentum dispersion is linear and the band gap is zero, such that electrons and holes, behave like Dirac fermions, i.e., relativistic particles with spin  $\frac{1}{2}$ . In graphene, the K and K' points are called the Dirac points [60,61]. Figure 2.2 shows the schematic of the band structure of monolayer graphene.

One of the notable properties of graphene that is obtained from experimental transport measurements is its remarkably high charge carrier mobility at room temperature, the values of which are reported in Table 1.1. Graphene exhibits a minimum conductivity on the order of  $4e^2/h$  near the neutrality point that depends on the impurity concentration in the graphene sheet [15,52]. Due to its excellent electronic properties graphene is a suitable candidate for wide range of potential applications, such as enhancing the strength of complex materials, high-speed analog electronics, etc.

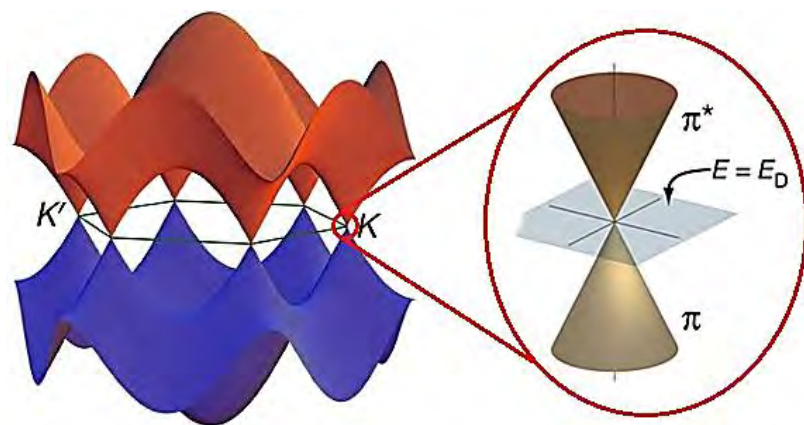


Figure 2.2 Schematic of the band structure of graphene, where two in-equivalent points, K and K', at the vertex of the Brillouin zone display no energy gap between two sublattices [62].

## 2.3 Applications

Potential applications for graphene are being seen and are under development in the fields of electronics, industrial processes, medicine, etc. Graphene with its unique physical, optical, and electronic properties has the potential to complement or replace silicon-based electronics as the properties of carbon allotropes such as carbon nanotubes or graphene can be controlled by the electric field [1,15]. Possible innovations of graphene-based electronic devices such as touchscreen technology, LCD displays, solar cells would open new possibilities in the world of technology owing the fact that graphene is ultra-thin, yet strong and transparent material [1]. Figure 2.3 shows areas of possible industrial and educational applications of graphene. Additionally to electronic applications, graphene could potentially be an efficient energy storage source in industrial engineering, such as in the production of ultra-capacitors where graphene could theoretically manage greater energy storage density due to its particularly high surface area to mass ratio [71].

Obtaining good quality graphene with improved growth, transfer, and fabrication methods will bring the feasibility of these and many other applications of graphene closer toward mass production and everyday life utility. Researchers in material science and nanotechnology along with engineering companies have already considered applying graphene in various areas of high performance computing and electronics devices.

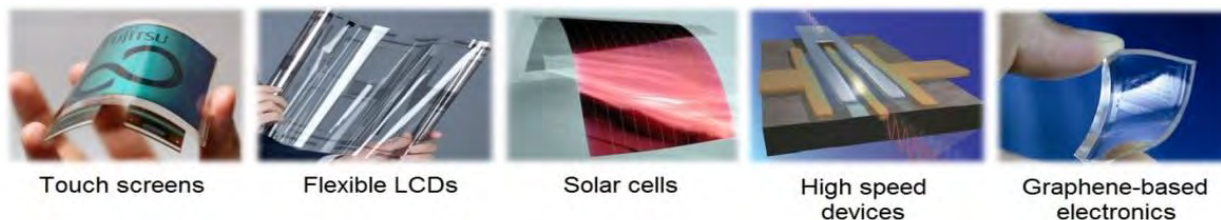


Figure 2.3 Potential graphene applications in industry and research.

### 3 GRAPHENE SYNTHESIS, TRANSFER, AND FABRICATION

Graphene has been synthesized in various ways and on different substrates. This section will summarize the synthesis methods of graphene and transfer techniques where appropriate. Each of the following fabrication techniques has its own advantages and limitations, as well as specific applications in research and industry.

#### 3.1 Exfoliated graphene

The scotch tape method denotes the micro-mechanical exfoliation of graphite using a piece of scotch tape [4,15]. During this process, adhesive tape is used to repeatedly split bulk graphite into thinner pieces, and the process is repeated until a single or few layers of graphite, i.e. graphene, is obtained. Using a dry deposition technique, the tape is pressed on a target substrate where fairly large crystallites of few micrometers to one millimeter in size are visible. Figure 3.1a illustrates the process of micro-mechanical cleavage of graphite, while Figure 3.1b shows the single layer graphene on the Si/SiO<sub>2</sub> substrate [4].

The method of micro-mechanical cleavage provides high structural and electronic quality material [4]. On the other hand, the pieces of exfoliated graphene are usually of several micrometers to few

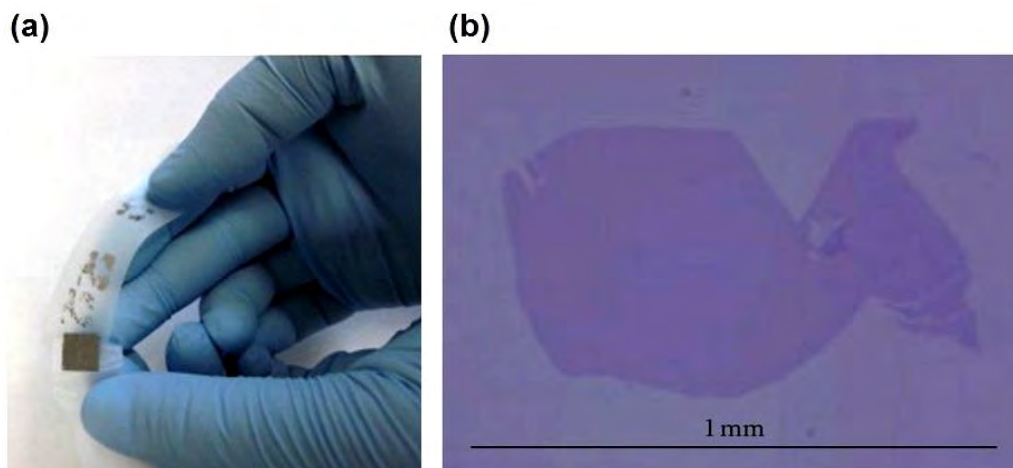


Figure 3.1 Exfoliated graphene: (a) process of mechanical exfoliation of graphene from bulk graphite using scotch tape, (b) single layer graphene transferred on SiO<sub>2</sub> wafer [4].

hundreds of micrometers is size, having irregular shapes and orientations. For graphene films being used in nanoelectronics and energy conversion, a scalable production is desired for industrial applications, much larger than the surface area of a single flake.

### 3.2 Epitaxial graphene on Silicon Carbide

Epitaxial graphene technique is a generally used to produce high quality monolayer graphene the surface area of which can reach few centimeters, depending on the size of the silicon carbide (SiC) wafer [16,18-20]. Heating SiC to high temperatures (1100 °C or greater) creates the desired conditions for some of the silicon to sublime, leaving a layer of carbon behind on the surface. The face of the SiC substrate used for graphene growth, i.e., silicon or carbon, determines the thickness, mobility, and carrier density of the resultant graphene. Figure 3.2 illustrates the faces of SiC and epitaxial graphene on the Si face of SiC (Figure 3.2a). Figure 3.2b shows an atomic force microscope (AFM) image of graphene/SiC terraces.

Graphene grown by the epitaxial method on SiC exhibits a similar electronic band-structure. Graphene on SiC also demonstrates the anomalous quantum Hall Effect associated with the properties of massless Dirac fermions. Even though the mobility of epitaxial graphene is not as great as that ob-

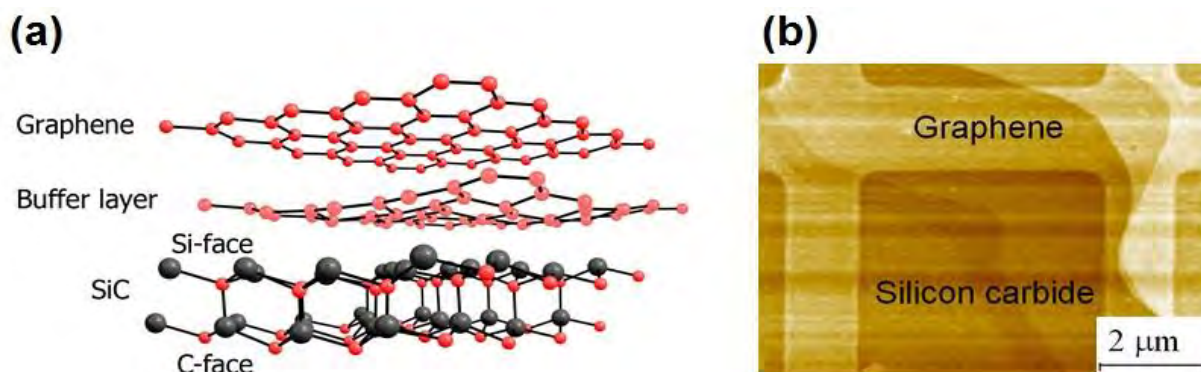


Figure 3.2 Epitaxial graphene on Silicon Carbide: (a) schematics of epitaxial graphene on silicon carbide showing buffer layer and Si- and C-termination [University of Groningen], (b) atomic force microscope (AFM) image of graphene/SiC terraces [NPL].



tained in exfoliated graphene, it has a major advantage in device application due to sizable surface area. Epitaxial graphene on SiC is to be utilized in production of large integrated electronics and in the production of high speed and high frequency transistors.

### 3.3 Chemical Vapor Deposition

The alternate technique to epitaxial growth of graphene is a CVD on catalytic metal substrate [7]. The CVD method became one of the most efficient ways to produce large-area and high quality graphene films. This method utilizes metal films of copper or nickel during chemical interaction between hydrogen or argon gas with carbon-containing gases due to the low solubility of carbon in these metals [5,6,21-27]. The growth is performed in a furnace heated to about 1000 °C at low pressure. Figure 3.3a shows the process of CVD growth where the hydrogen aids the reaction between methane and catalytic substrate during which process carbon atoms are chemically adsorbed on the metal surface. A fast cooling rate of the substrate is essential for the purpose of avoidance of carbon aggregation into bulk graphite on top of the metal film. The CVD method of graphene growth utilizes the foils of copper and nickel, where mono- or few-layer graphene can be grown. The growth of graphene on copper foils can form single-layer graphene, whereas with nickel substrates multi-layer films are formed through carbon segregation, precipitation, and absorption. Copper became the optimal choice for the catalytic substrate due to the extremely low solubility of carbon in copper that allows production of monolayer graphene with a high percentage of single layers. Figure 3.3b demonstrates the SEM image of graphene on copper foil. After the chemical deposition of graphene on the metal catalyst is complete, the graphene can be transferred to diverse substrates, as seen from Figure 3.3c. This feature makes the CVD method suitable for many applications.

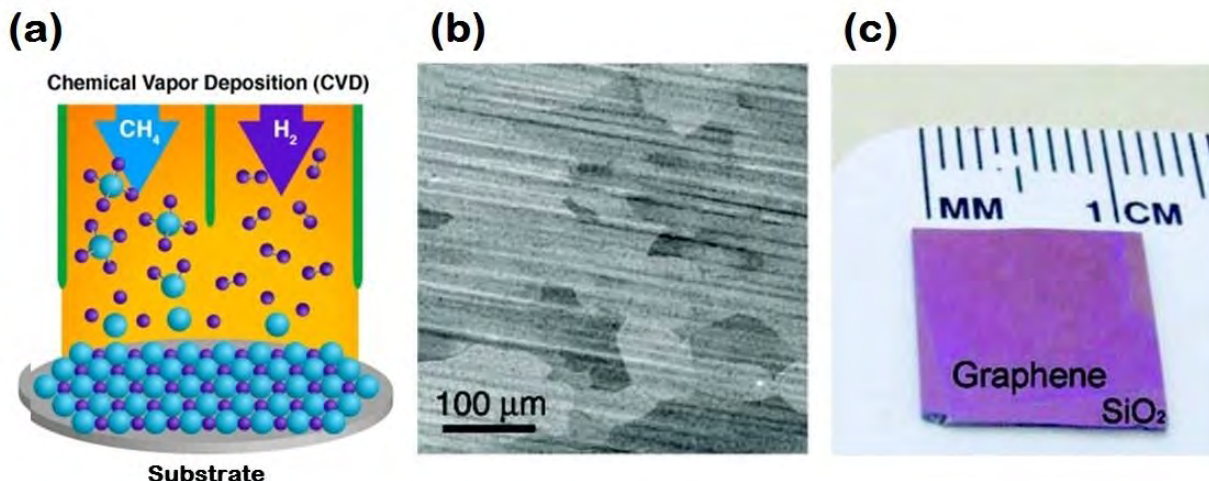


Figure 3.3 Graphene synthesized by CVD. (a) CVD growth process, where hydrogen atoms support the reaction between methane and catalytic substrate during which process carbon atoms are chemically adsorbed on the metal surface [MMU Research, The Dalton Research Institute]. (b) SEM image of CVD graphene on copper substrate with copper striations and grain boundaries are clearly visible [7]. (c) CVD graphene transferred onto  $\text{SiO}_2$  substrate after copper has been chemically removed [7].

### 3.3.1 Transfer methods

Among the many possible transfer techniques, polymer aided transfer is mostly used. Transfer processes have been demonstrated using wet and dry transfer via polymer aid such as PMMA, polydimethylsiloxane (PDMS) frames or elastomer stamps [13,63]. PMMA is commonly utilized mechanical support for graphene transfer. First, PMMA is spin coated on top of graphene on Cu, after which Cu is etched away using ferric nitrite ( $\text{Fe}(\text{NO}_3)_3$ ) or ferric chloride ( $\text{FeCl}_3$ ) solution. Then the graphene with polymer is thoroughly rinsed in deionized water and placed carefully on the top of the target substrate. Once the graphene/polymer membrane is dry, an acetone or dichloromethane bath is commonly used to remove a layer of PMMA. The transfer process for the polymer supported graphene is shown in Figure 3.4.

After copper has been chemically removed via the process illustrated on Figure 3.4, the quality of graphene and the number of graphene layers can be evaluated using Raman spectroscopy. In Raman spectroscopy, a spot on the sample is illuminated with a laser beam of fixed wavelength. The light from

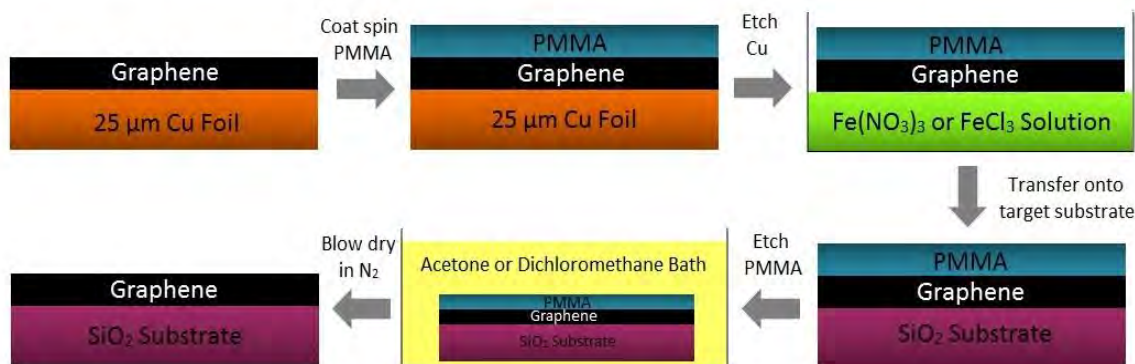


Figure 3.4 Schematic illustration of wet transfer process of CVD grown graphene on copper foil onto SiO<sub>2</sub> substrate.

the target spot is then collected with a lens and sent through a monochromator where some of the out and the rest are dispersed onto a detector to produce a spectrum of the surface. Figure 3.5b [64] shows typical Raman spectrum of single-, double-, and multi-layer graphene synthesized by CVD on copper and transferred to the SiO<sub>2</sub> substrate, as shown on Figure 3.5a.

The intensity of Raman D band ( $\sim 1350\text{ cm}^{-1}$ ) in graphene determines the defect density. In Figure 3.5b, the  $I_{2D}/I_G$  intensity ratio of the spectrum is about 2 indicating that the graphene is a single layer; the blue curve on Figure 3.5b represents a bilayer graphene, with  $I_{2D}/I_G \approx 1$ ; the black curve corresponds to multi-layer graphene where  $I_{2D}/I_G < 1$ . The Raman spectrum of CVD graphene can also be taken directly while on the catalytic substrate after the growth has been completed.

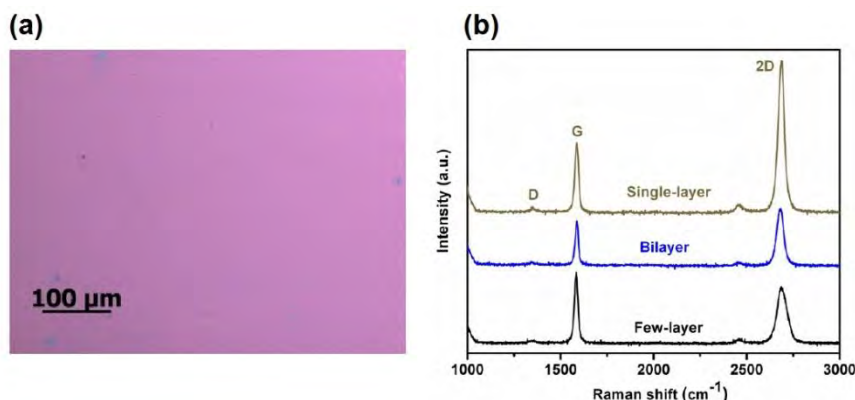


Figure 3.5 (a) Optical micrograph of CVD graphene on SiO<sub>2</sub> substrate [1], (b) Raman spectroscopy of the transferred graphene on SiO<sub>2</sub> substrate in image (a) illustrating the presence of single-layer (brown curve), bilayer (blue curve), and few-layer graphene (black curve) with identified D, G, and 2D peaks [64].

## 4 EXPERIMENTAL CHARACTERIZATIONS AND RESULTS<sup>2</sup>

### 4.1 Copper foil annealing process

25  $\mu\text{m}$  thick copper foils were annealed using a horizontal 1 inch quartz tube furnace system. The experimental schematics and furnace setup are illustrated in Figure 4.1. The system is first pumped down to a base pressure of 36 mTorr. Then, the furnace is heated to 1025  $^{\circ}\text{C}$  with 10 sccm flow of  $\text{H}_2\text{N}_2$  reaching 200 mTorr  $\text{H}_2\text{N}_2$  pressure. Once the temperature reached 1025  $^{\circ}\text{C}$ , the flow of  $\text{CH}_4$  is introduced to the system. Both  $\text{CH}_4$  with 40 sccm and  $\text{H}_2\text{N}_2$  with 10 sccm are flowing during the process at 1025  $^{\circ}\text{C}$  for 30 min ( $P \sim 500$  mTorr). After heat treatment, the specimens were cooled to room temperature over a period of two hours. The thermal and chemical treatments of copper foils are described in Table 4.1.

The label at the top right corner of the images in Figures 4.2 – 4.9 indicates the protocol to which the specimen was subjected. BF indicates bare foil, EF (etched foil) denotes foils etched in  $\text{Fe}(\text{NO}_3)_3$  for 30 seconds,  $\text{H}_2\text{N}_2$  signifies heat treatment in forming gas at 1025  $^{\circ}\text{C}$  for 30 minutes, and  $\text{H}_2\text{N}_2:\text{CH}_4$  marks heat treatment in forming gas and methane at 1025  $^{\circ}\text{C}$  for 30 minutes. For all the heat treatment protocols, the furnace with the Cu foil required a period of 30 minutes to reach the operating

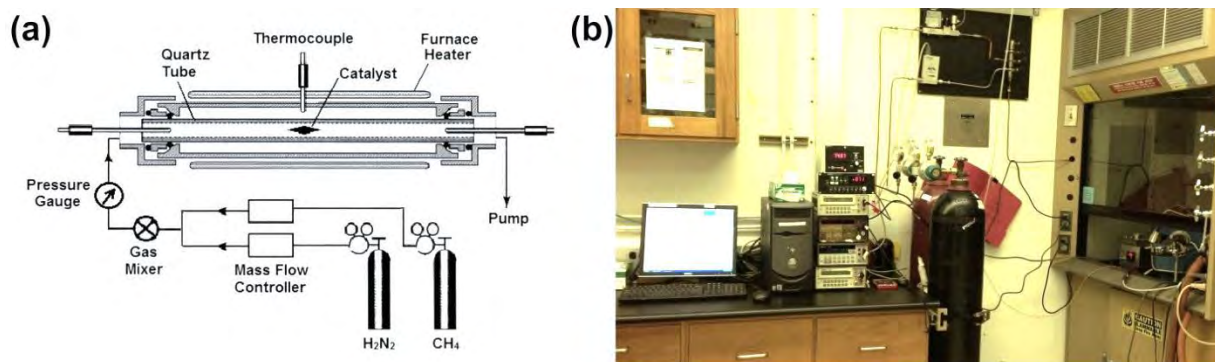


Figure 4.1 (a) Schematics of the CVD system. (b) Photo of the experimental set-up of CVD growth furnace.

<sup>2</sup> The contents in this chapter were published in Chemistry of Materials: Sarajlic, O. I.; Mani, R. G. "Mesoscale Scanning Electron and Tunneling Microscopy Study of the Surface Morphology of Thermally Annealed Copper Foils for Graphene Growth". Chem. Mater. **2013**, 25, 1643–1648. Copyright belongs to American Chemical Society, Chemistry of Materials.

Table 4.1 Description of the protocols applied to the unetched bare foil (BF) and the etched foil (EF) of copper.

Bare Foil (BF)	Etched Foil (EF)
<b>BF:</b> 25 $\mu\text{m}$ Cu foil	<b>EF:</b> 25 $\mu\text{m}$ Cu foil etched in $\text{Fe}(\text{NO}_3)_3$
<b>BF+H<sub>2</sub>N<sub>2</sub></b> 25 $\mu\text{m}$ Cu foil heat treated in H <sub>2</sub> N <sub>2</sub> [10 sccm] at 1025°C for 30 minutes (P~200mTorr)	<b>EF+H<sub>2</sub>N<sub>2</sub></b> 25 $\mu\text{m}$ etched Cu foil and heat treated in H <sub>2</sub> N <sub>2</sub> [10 sccm] at 1025°C for 30 minutes (P~200mTorr)
<b>BF+(H<sub>2</sub>N<sub>2</sub>:CH<sub>4</sub>)</b> 25 $\mu\text{m}$ Cu foil heat treated in H <sub>2</sub> N <sub>2</sub> :CH <sub>4</sub> [10 sccm : 40 sccm] at 1025°C for 30 minutes (P~500mTorr)	<b>EF+(H<sub>2</sub>N<sub>2</sub>:CH<sub>4</sub>)</b> 25 $\mu\text{m}$ etched Cu foil heat treated in H <sub>2</sub> N <sub>2</sub> :CH <sub>4</sub> [10 sccm : 40 sccm] at 1025°C for 30 minutes (P~500mTorr)
<b>BF+H<sub>2</sub>N<sub>2</sub>+(H<sub>2</sub>N<sub>2</sub>:CH<sub>4</sub>)</b> 25 $\mu\text{m}$ Cu foil heat treated sequentially, first in H <sub>2</sub> N <sub>2</sub> [10 sccm] at 1025°C for 30 minutes (P~200mTorr) then in H <sub>2</sub> N <sub>2</sub> :CH <sub>4</sub> [10 sccm : 40 sccm] at 1025°C for 30 minutes (P~500mTorr)	<b>EF+H<sub>2</sub>N<sub>2</sub>+(H<sub>2</sub>N<sub>2</sub>:CH<sub>4</sub>)</b> 25 $\mu\text{m}$ etched Cu foil heat treated sequentially, first in H <sub>2</sub> N <sub>2</sub> [10 sccm] at 1025°C for 30 minutes (P~200mTorr) then in H <sub>2</sub> N <sub>2</sub> :CH <sub>4</sub> [10 sccm : 40 sccm] at 1025°C for 30 minutes (P~500mTorr)

temperature of 1025 °C. During this warm-up period, there was a constant 10 sccm flow of H<sub>2</sub>N<sub>2</sub> in the quartz tube. These protocols were chosen because they often appear in recipes for CVD graphene.

## 4.2 Optical Characterizations

After the foils were annealed using the protocols described in Table 4.1, they were characterized using Optical Microscopy (OM), Scanning Tunneling Microscopy (SEM), and Scanning Tunneling Microscopy (STM) to show the evolution of the surface morphology after every pre-treatment and/or pre-annealing procedure.

### 4.2.1 Optical Microscopy

Figures 4.2 – 4.5 exhibit optical microscope images. We begin by looking at the bare Cu foil (BF) surface. Figure 4.2a shows pronounced striations, which are the parallel lines rotated slightly clockwise with respect to the vertical, going across the surface of the substrate. Such striations are believed to result from the rolling of copper into foil at high pressure. Then the foil was etched in the  $\text{Fe}(\text{NO}_3)_3$  (1M)



solution for 30 seconds (Figure 4.2b). Here, the aim was to remove the striations and fractures/dents, and smoothen the bare foil surface. Instead, the foil developed a coarse texture with etch pits after the etch.

Figure 4.3a shows an optical image where a 250  $\mu\text{m}$  wide Cu grain, with nearly horizontal striations below, is clearly visible in the Cu foil annealed under  $\text{H}_2\text{N}_2$  for 30 minutes at 1025  $^\circ\text{C}$ . This protocol represents the typical pre-annealing procedure utilized to prepare the foil surface, prior to the introduction of methane. This protocol also visibly removes the native copper oxide, via the chemical reduction of the oxidized copper by hydrogen. The successive application of both the  $\text{Fe}(\text{NO}_3)_3$  etch and the  $\text{H}_2\text{N}_2$  anneal to the Cu foil creates a rolling terrain with surface scarring visible at low magnification as seen from Figure 4.3b.

Figure 4.4a displays un-etched foil exposed to a  $\text{H}_2\text{N}_2:\text{CH}_4$  for 30 minutes at 1025  $^\circ\text{C}$ , where the Cu grain boundary is also clearly pronounced. After the Cu foils were etched and subjected to  $\text{H}_2\text{N}_2:\text{CH}_4$  at 1025  $^\circ\text{C}$ , as illustrated on Figure 4.4b, the scarred Cu surface with micron sized pits and dents were covered with monolayer graphene film.

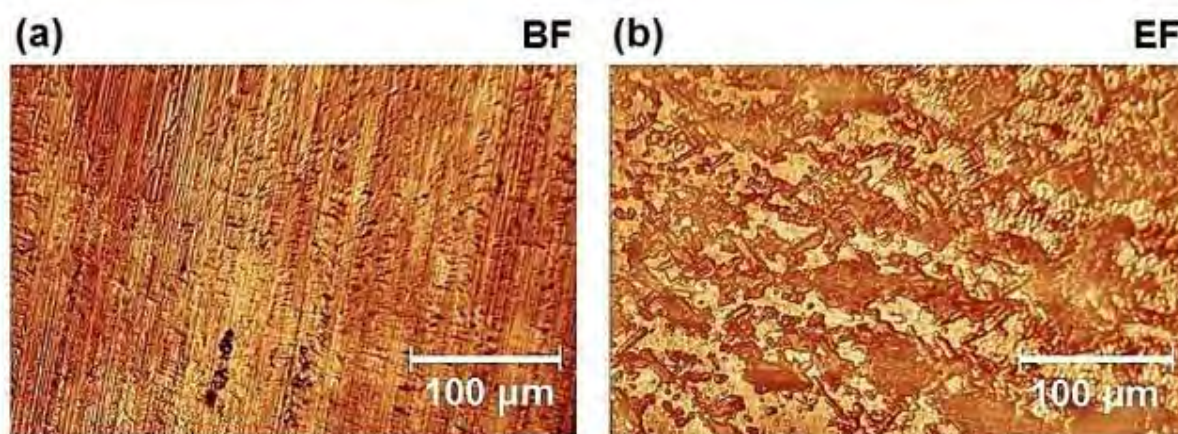


Figure 4.2 Optical images of 25  $\mu\text{m}$  Cu foil at 400 $\times$  magnification. The label at the top right of the images indicates the protocol to which the specimen was subjected, see also Table 4.1. BF indicates bare foil, EF indicates etched foil. (a) This panel shows that bare foil includes striations resulting from rolling copper at high pressure. (b) Bare foil subjected to a  $\text{Fe}(\text{NO}_3)_3$  etch produces a nonuniform surface with micrometer sized pores.

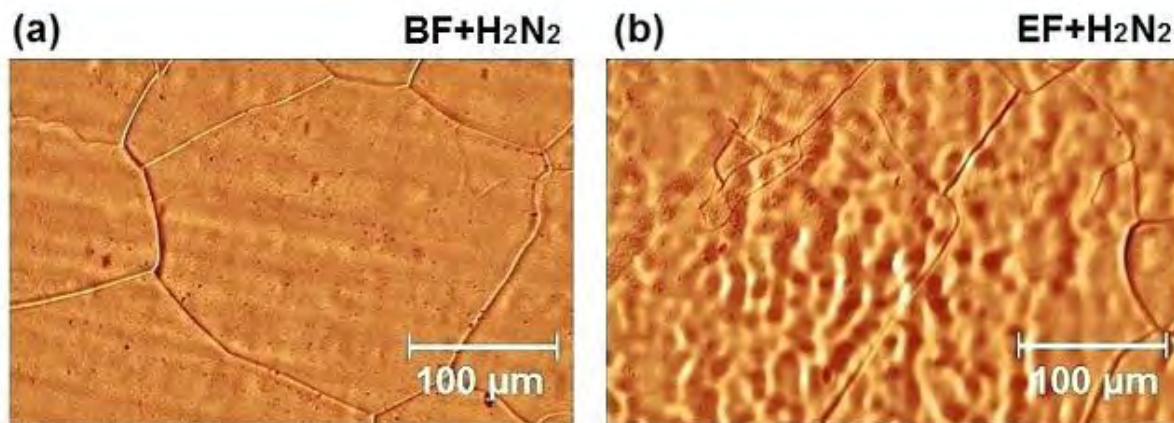


Figure 4.3 Optical images of 25  $\mu\text{m}$  Cu foil at 400 $\times$  magnification. The label at the top right of the images indicates the protocol to which the specimen was subjected, see also Table 4.1. BF indicates bare foil, EF indicates etched foil,  $\text{H}_2\text{N}_2$  indicates heat treatment in forming gas at 1025  $^\circ\text{C}$  for 30 min. (a) Bare Cu foil heat treated in  $\text{H}_2\text{N}_2$  at 1025  $^\circ\text{C}$  for 30 min displays a 250  $\mu\text{m}$  wide copper grain along with traces of striations that are less pronounced after thermal treatment. (b) Etched foil treated in  $\text{H}_2\text{N}_2$  at 1025  $^\circ\text{C}$  for 30 min displays few hundred micrometer wide grains with surface scars.

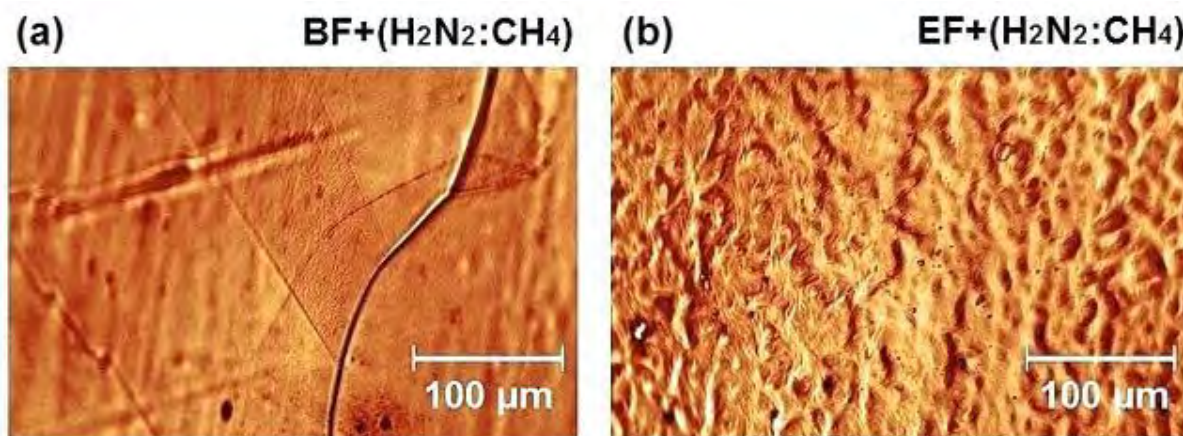


Figure 4.4 Optical images of 25  $\mu\text{m}$  Cu foil at 400 $\times$  magnification. The label at the top right of the images indicates the protocol to which the specimen was subjected, see also Table 4.1. BF indicates bare foil, EF indicates etched foil,  $\text{H}_2\text{N}_2$  indicates heat treatment in forming gas at 1025  $^\circ\text{C}$  for 30 min, and  $\text{H}_2\text{N}_2:\text{CH}_4$  indicates heat treatment in forming gas and methane at 1025  $^\circ\text{C}$  for 30 min. (a) Bare foil thermally exposed to  $\text{H}_2\text{N}_2:\text{CH}_4$  shows graphene on top of copper grains. Here, vertical striations are still visible in the underlying copper foil. (b) Etched foil heat treated under  $\text{H}_2\text{N}_2:\text{CH}_4$  at 1025  $^\circ\text{C}$  for 30 min indicates indistinct Cu grains covered with a single layer of graphene. Also visible are micrometer sized pits and dents.

The last protocol is intended to answer whether pre-annealing the Cu surface before flow of methane gas improves the catalytic surface for graphene growth. Therefore, Figure 4.5a shows the optical image of Cu foil subjected to pre-annealing under  $\text{H}_2\text{N}_2$  for 30 minutes followed by  $\text{H}_2\text{N}_2:\text{CH}_4$  expo

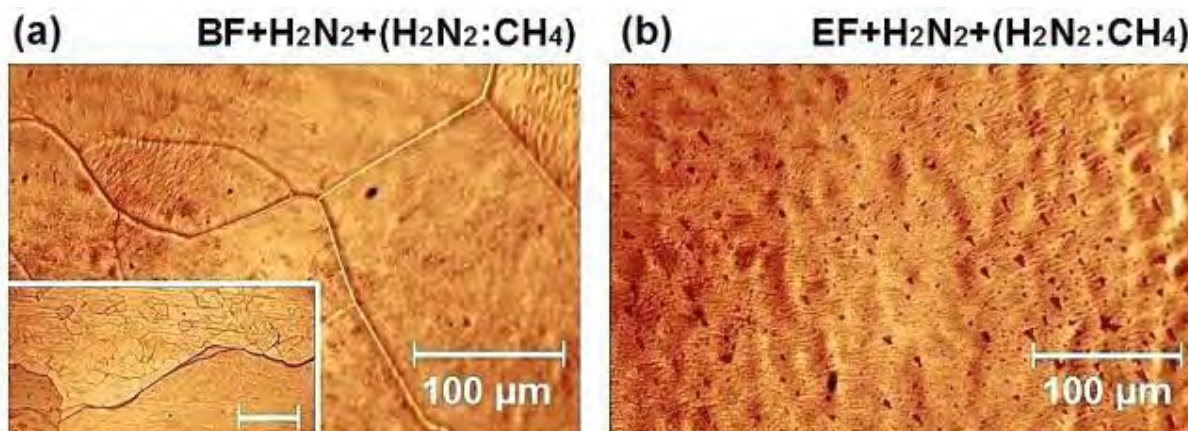


Figure 4.5 Optical images of 25  $\mu\text{m}$  Cu foil at 400 $\times$  magnification. The label at the top right of the images indicates the protocol to which the specimen was subjected, see also Table 4.1. BF indicates bare foil, EF indicates etched foil,  $\text{H}_2\text{N}_2$  indicates heat treatment in forming gas at 1025  $^\circ\text{C}$  for 30 min, and  $\text{H}_2\text{N}_2:\text{CH}_4$  indicates heat treatment in forming gas and methane at 1025  $^\circ\text{C}$  for 30 min. (a) Bare foil subjected to heat treatment under  $\text{H}_2\text{N}_2$  at 1025  $^\circ\text{C}$  for 30 min followed by  $\text{H}_2\text{N}_2:\text{CH}_4$  at 1025  $^\circ\text{C}$  for 30 min displays single layer graphene film overlying Cu grains that are a few hundreds micrometers wide. Inset: A partially peeled Cu foil (scale bar is 500  $\mu\text{m}$ ) that lost the crust layer. (b) Etched foil subjected to heat treatment under  $\text{H}_2\text{N}_2$  at 1025  $^\circ\text{C}$  for 30 min followed by  $\text{H}_2\text{N}_2:\text{CH}_4$  at 1025  $^\circ\text{C}$  for 30 min shows less surface nonuniformity and includes monolayer graphene.

sure for another 30 minutes at 1025  $^\circ\text{C}$ . This protocol results in crusting, with Cu grains on the crust, and the peeling of crust layers of Cu foil along with graphene (see insert Figure 4.5a). However, in unpeeled areas, grains of Cu covered with monolayer graphene were clearly perceptible. Figure 4.5b demonstrates that annealing with  $\text{H}_2\text{N}_2$  and  $\text{H}_2\text{N}_2:\text{CH}_4$  smoothen out the non-uniformity of the surface, leaving micron sized pits still visible, as the Cu foil is covered by mono-layer graphene. Therefore, the optical study of Cu foils shows that exposing the bare Cu foil to both  $\text{H}_2\text{N}_2:\text{CH}_4$  and  $\text{H}_2\text{N}_2+(\text{H}_2\text{N}_2:\text{CH}_4)$  protocols produces monolayer graphene.

#### 4.2.2 Scanning Electron Microscopy

We examined the same Cu foils with SEM. As in the optical image of Figure 4.2a, Figure 4.6a confirms (vertical) striations on Cu in the SEM image. However, the SEM image also shows horizontally running surface fractures/dents. Figure 4.6b does not show striations or fractures on the Cu surface as the  $\text{Fe}(\text{NO}_3)_3$  etch leaves behind a coarse surface.



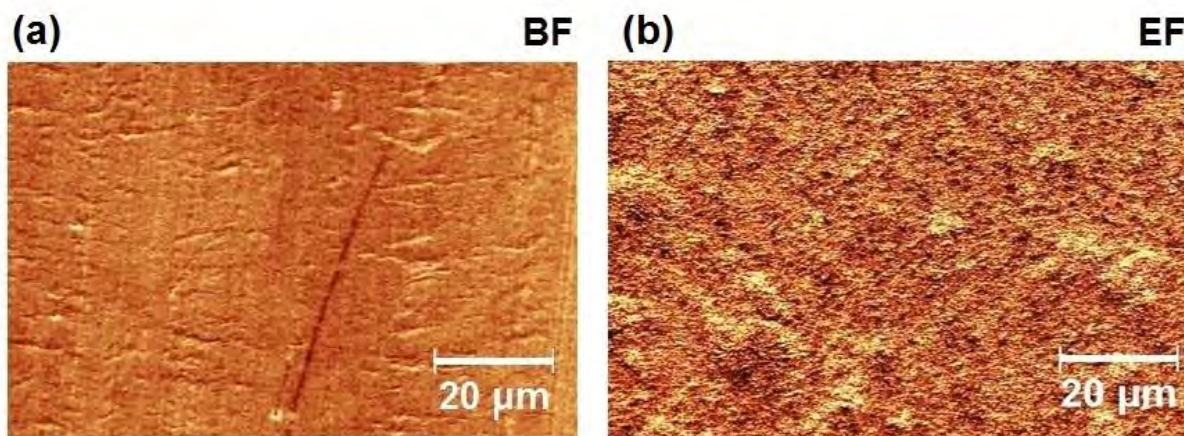


Figure 4.6 SEM images of 25  $\mu\text{m}$  Cu foil. The label at the top right of the images indicates the protocol to which the specimen was subjected, see also Table 4.1. BF indicates bare foil, EF indicates etched foil. (a) Striations resulting from rolling copper at high pressure are still visible in the SEM image. Also visible are microscopic dents/fractures in the foil surface. (b) Bare foil subjected to a  $\text{Fe}(\text{NO}_3)_3$  etch produces a nonuniform surface with etch quarries encrusted onto the surface.

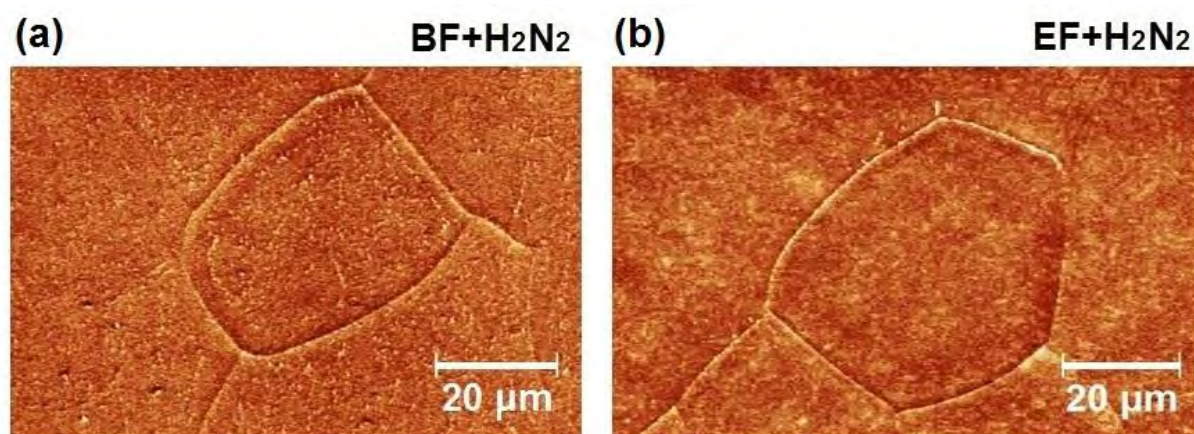


Figure 4.7 SEM images of 25  $\mu\text{m}$  Cu foil. The label at the top right of the images indicates the protocol to which the specimen was subjected, see also Table 4.1. BF indicates bare foil, EF indicates etched foil,  $\text{H}_2\text{N}_2$  indicates heat treatment in forming gas at 1025  $^\circ\text{C}$  for 30 min. (a) Heat treated bare Cu foil displays an approximately 50  $\mu\text{m}$  wide grain. (b) Etched foil heat treated under  $\text{H}_2\text{N}_2$  also displays an approximately 50  $\mu\text{m}$  wide grain.

Figure 4.7a clearly illustrates presence of Cu grains and grain boundaries. The exhibited grain at the center of the figure is about 50  $\mu\text{m}$  wide in this  $\text{H}_2\text{N}_2$  annealed foil. Etched foil heat treated in  $\text{H}_2\text{N}_2$  as seen from Figure 4.7b still displays Cu grain boundaries. Here, the grain at the center is about 50  $\mu\text{m}$  wide. A close examination still indicates coarseness in the surface although it is now significantly reduced.

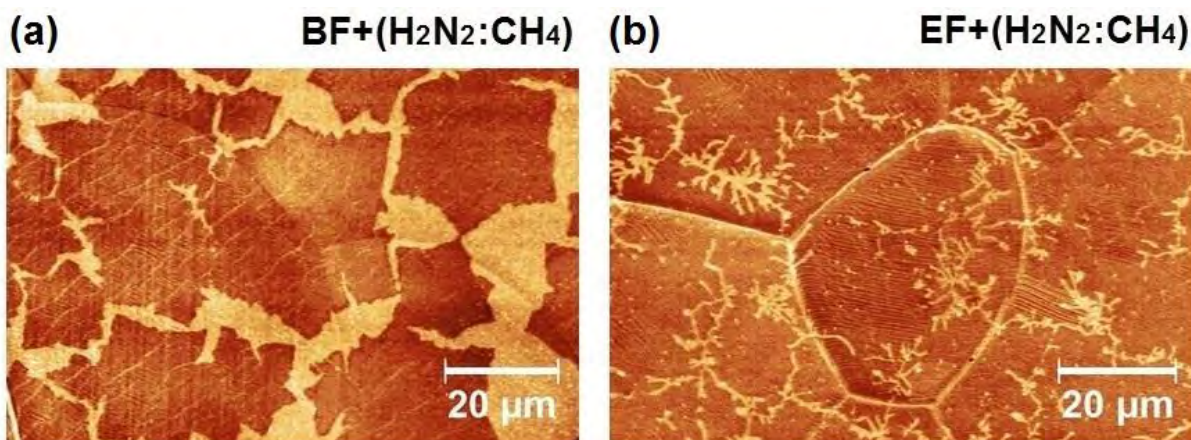


Figure 4.8 SEM images of 25  $\mu\text{m}$  Cu foil. The label at the top right of the images indicates the protocol to which the specimen was subjected, see also Table 4.1. BF indicates bare foil, EF indicates etched foil,  $\text{H}_2\text{N}_2$  indicates heat treatment in forming gas at 1025  $^\circ\text{C}$  for 30 min, and  $\text{H}_2\text{N}_2:\text{CH}_4$  indicates heat treatment in forming gas and methane at 1025  $^\circ\text{C}$  for 30 min. (a) Well pronounced 20–30  $\mu\text{m}$  wide flower-shaped structures are observed on the surface of copper once the Cu foil has been treated with  $\text{H}_2\text{N}_2:\text{CH}_4$ . Vertically running striations are still evident on the left. These flower structures suggest graphene grains that have not yet coalesced into a uniform and continuous sheet of graphene. (b) This panel shows graphene domains, with multiple wrinkles within them, that are on the verge of coalescing together to cover the underlying metallic substrate.

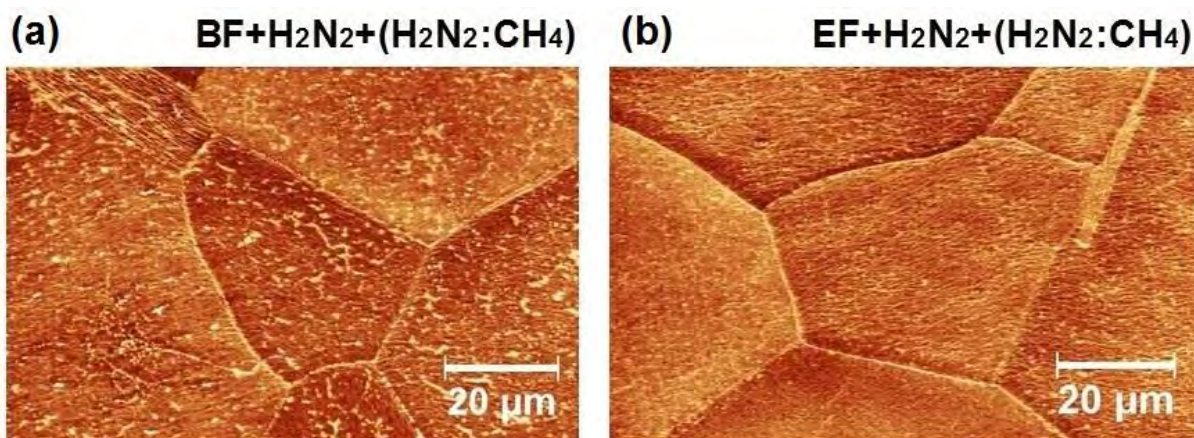


Figure 4.9 SEM images of 25  $\mu\text{m}$  Cu foil. The label at the top right of the images indicates the protocol to which the specimen was subjected, see also Table 4.1. BF indicates bare foil, EF indicates etched foil,  $\text{H}_2\text{N}_2$  indicates heat treatment in forming gas at 1025  $^\circ\text{C}$  for 30 min, and  $\text{H}_2\text{N}_2:\text{CH}_4$  indicates heat treatment in forming gas and methane at 1025  $^\circ\text{C}$  for 30 min. (a) This figure shows the Cu surface nearly fully covered with graphene. (b) The image shows the graphene layer overlying micrometer sized pits in the etched Cu foil.

Once the Cu foil has been treated with  $\text{H}_2\text{N}_2:\text{CH}_4$  (Figure 4.8a), well pronounced with approximately 20 - 30  $\mu\text{m}$  wide flower-shaped structures are observed on the surface of copper, although vertically running striations are still evident towards the left of the figure. These structures suggest graphene



grains that have not yet coalesced into a uniform and continuous sheet of graphene. Remarkably, the graphene grains show indications of crossing Cu grain boundaries. This can be seen in the left-half of Figure 4.8a, where a semi-circular grain boundary cuts through at least two graphene grains. Figure 4.8b shows wrinkled graphene domains. These domains appear to be on the verge of coalescing together to cover the underlying substrate. Note that Figure 4.3c shows more perceptible flower-shaped structures in comparison to Figure 4.8b, where the light shaded regions of copper resemble stitch marks between graphene domain boundaries.

Figure 4.9a shows the Cu surface nearly fully covered with graphene after the  $H_2N_2 + (H_2N_2:CH_4)$  protocol. The image on Figure 4.9b shows the graphene layer overlying micron sized pits in the etched Cu foil. Thus, it appears that both the  $BF+(H_2N_2:CH_4)$  and the  $EF+(H_2N_2:CH_4)$  protocols offer a desirable environment for graphene growth.

Each method has its advantages: the growth on BF produces individual flower-shaped structures or disconnected patches of graphene, while growth by the  $EF+(H_2N_2:CH_4)$  protocol appears to be a faster approach to producing continuous graphene films.

### 4.2.3 Scanning Tunneling Microscopy

Some results from the Scanning Tunneling Microscope (STM) study are shown in Figures 4.10 – 4.12. Figure 4.10a shows the STM image of bare Cu foil consisting of a granular Cu surface with average grain diameter of about 20 nm. The cross-sectional profile as seen from Figure 4.10b provides important information about the roughness of the surface after a specific course of treatment. From many parameters that describe roughness, average roughness ( $R_a$ ) gives the vertical deviations of the actual surface topography from its smooth form inside an evaluation length, divided by the number of points in the cross-section [65],

$$Ra = \frac{1}{N} \sum_{j=1}^N |r_j|.$$

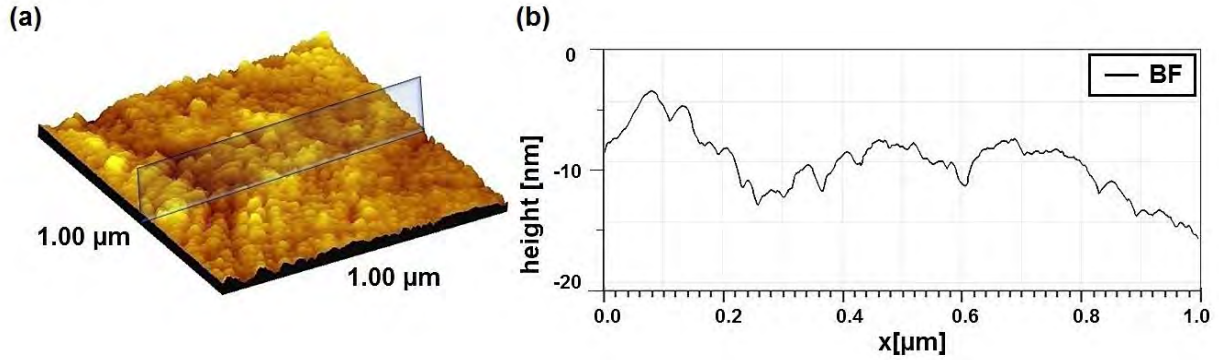


Figure 4.10 (a) STM image of bare Cu foil that shows a granular surface with average grain diameter of about 20 nm. (b) This figure shows a 10 nm height variation in the bare foil over a 0.2 μm interval in the domain  $0 \leq x \leq 0.3$  μm, with  $R_a = 0.25$  nm over the line trace.

Here,  $r_j$  is the vertical distance from the mean line to the  $j^{th}$  data point. The cross-sectional surface profile of BF in Figure 4.10b shows a 10 nm height variation over a 0.2 μm interval in the domain  $0 \leq x \leq 0.3$  μm, with  $R_a = 0.25$  nm over the line trace.

STM image of un-etched Cu foil exposed to  $H_2N_2$  at 1025 °C is shown on Figure 4.11a. Under thermal annealing in  $H_2N_2$ , the overall end-to-end height variation on Figure 4.11b is only 3 nm suggesting that the Cu surface flattens, and the average roughness of the Cu foil is  $R_a = 0.18$  nm. Figure 4.12a displays the STM image of bare foil heat treated with  $H_2N_2:CH_4$ . This figure shows stripe-like features that correspond to the graphene wrinkles observed by SEM, see Figure 4.8. Thus, Figure 4.12a exhibits a continuous graphene layer over the Cu substrate. To confirm this point, the insert of Figure 4.12a displays an atomic resolution image of graphene on polycrystalline Cu. In contrast to cross-sectional profiles displayed on Figures 4.10b and 4.11b, in Figure 4.12b, there is a 10 nm height difference from one end of the cross section to the other, with  $R_a = 0.08$  nm. Therefore, surface roughness of Cu film is significantly reduced after exposing it to  $H_2N_2:CH_4$ . Perhaps, the reason for this result is that the overlying graphene layer is smoother.

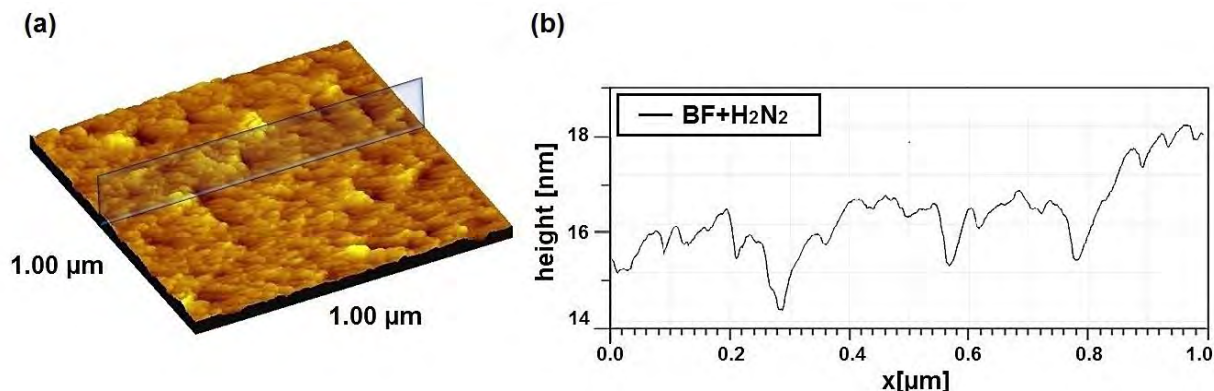


Figure 4.11 (a) STM image of unetched Cu foil exposed to  $\text{H}_2\text{N}_2$ . The grains appear to be flattened. (b) Cross-sectional profile showing 3 nm height variation with average surface roughness of 0.18 nm in the  $\text{H}_2\text{N}_2$  annealed foil.

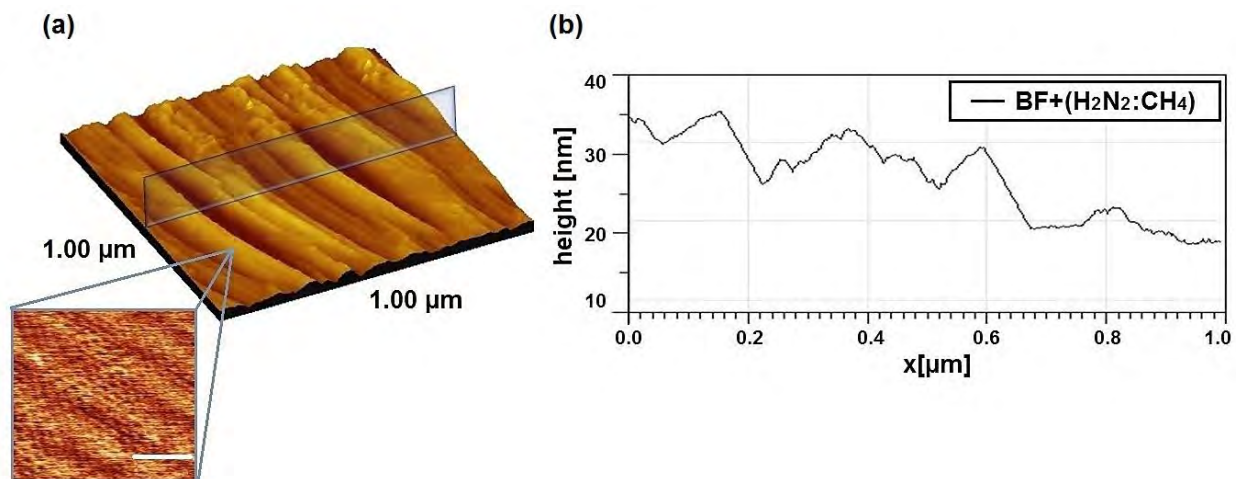


Figure 4.12 (a) STM image of unetched Cu foil heat treated in  $\text{H}_2\text{N}_2:\text{CH}_4$  for 30 min at 1025 °C. This protocol produces a monolayer graphene sheet that covers the underlying catalytic substrate. Inset: Atomic resolution image of graphene on copper (scale bar is 2 nm). (b) Cross-sectional profile showing 10 nm height variations with average surface roughness of 0.08 nm in  $\text{H}_2\text{N}_2:\text{CH}_4$  treated foil.

### 4.3 Transfer process

After the CVD growth of graphene on copper foil is cooled down, a polymer deposited on top of graphene can serve as a transfer aid. The Poly(methyl methacrylate) (PMMA) transfer method was utilized as a supporting mechanical substrate. The PMMA solution was spin-coated onto the graphene/Cu substrate, softly baked for 5 minutes at 100 °C, then chemical etched with  $\text{Fe}(\text{NO}_3)_3$  etching (1M) solution. Silicon dioxide ( $\text{SiO}_2$ ) served as a substrate of choice for graphene/polymer system. The transfer process of graphene from graphene/copper foil onto  $\text{SiO}_2$  substrate is illustrated on Figure 4.13.

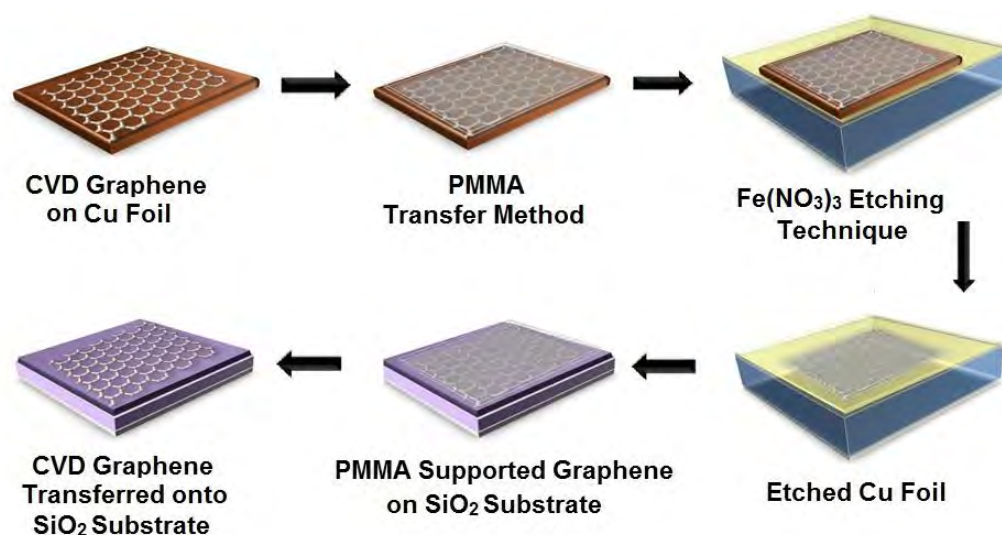


Figure 4.13 Schematic diagram of graphene transfer procedure onto silicon dioxide substrate.

Once graphene is etched from the catalytic substrate, it can be placed on a target substrate such as oxidized silicon wafer, glass, muscovite mica, or sapphire. Si/SiO<sub>2</sub> wafer is commonly used substrate for graphene deposit. Having a thin carbon layer firmly attached to the surface of Si/SiO<sub>2</sub> substrate by weak van der Waals forces allows investigating the homogeneity of resultant graphene films as a function of the growth conditions. Thus, growth, transfer, and fabrication of graphene films are essential and inter-related steps toward enhancement of complex materials and production of high-speed electronics.

#### 4.4 Raman Spectrum

Figure 4.14a is an optical micrograph of the graphene film realized with the H<sub>2</sub>N<sub>2</sub>:CH<sub>4</sub> protocol. The Cu foil with graphene that is shown in Figures 4.4a and 4.8a was etched in Fe(NO<sub>3</sub>)<sub>3</sub> and transferred to SiO<sub>2</sub> wafer using a Poly(methyl methacrylate) (PMMA) liftoff method. Comparing the textures of the transferred graphene film (Figure 4.14a) and the Cu foil surface (Figures 4.4a and 4.8a), we see that the graphene film preserves an imprint of the Cu foil grain structure, as the darker regions in the graphene correspond to the grain boundaries seen in the Cu surface. Here, it appears that the deeper the grain boundary structure of the Cu foil, the more pronounced are the contrast variations in the transferred

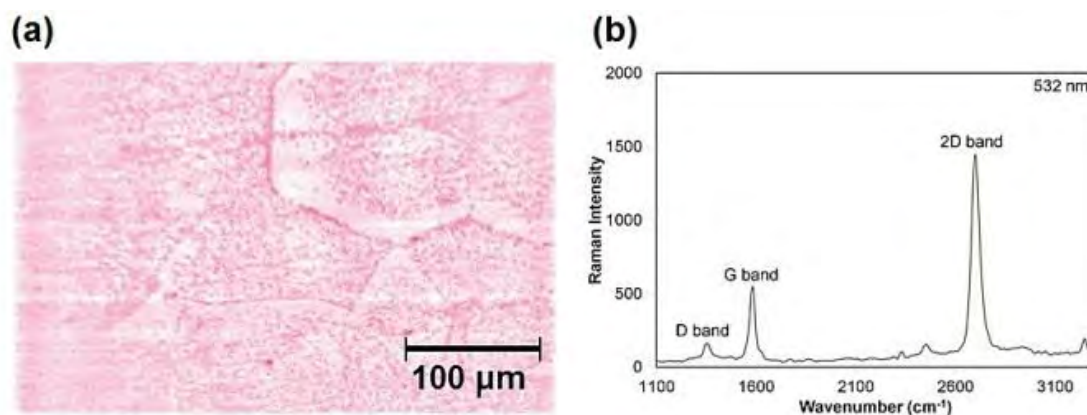
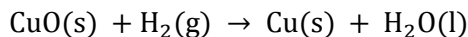


Figure 4.14 (a) Cu foil with graphene (see Figures 4.4a and 4.8a) was etched with  $\text{Fe}(\text{NO}_3)_3$  and transferred onto  $\text{SiO}_2$  wafer using a PMMA transfer technique. Here, traces of Cu grain boundaries appear to be imprinted on the graphene layer. (b) Raman spectrum of the graphene film obtained with 532 nm laser excitation.

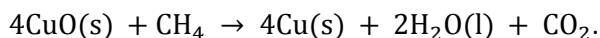
graphene film. A Raman spectrum of the transferred graphene suggests mostly single layer graphene based on the intensity ratio between 2D peak with frequency of  $2700 \text{ cm}^{-1}$  and the G band of  $\sim 1580 \text{ cm}^{-1}$  (Figure 4.14). The Raman D band which is located at  $\sim 1350 \text{ cm}^{-1}$  represents defects in graphene due to the inelastically scattered zone-boundary phonons that do not satisfy the Raman selection rule [66,67]. This feature is attributed to the Cu grain boundaries [36] which are replicated in the transferred graphene film as illustrated on Figure 4.14a.

## 5 EFFECTS ON COPPER SURFACE MORPHOLOGY: DISCUSSION<sup>3</sup>

Bare copper foil is often covered with copper oxide. At elevated temperatures, the relevant reactions for the reduction of copper oxide are



and



Reduction of copper oxide by hydrogen ( $\text{H}_2$ ) is known to be faster than reduction by methane ( $\text{CH}_4$ ). Thus, in the utilized protocols, BF (or EF) +  $\text{H}_2\text{N}_2$ , should be very effective in reducing the oxide. BF (or EF) +  $\text{H}_2\text{N}_2$  + ( $\text{H}_2\text{N}_2\text{:CH}_4$ ) should be even more so since there is exposure to the  $\text{H}_2\text{N}_2$  and  $\text{CH}_4$  during graphene growth. The BF (or EF) + ( $\text{H}_2\text{N}_2\text{:CH}_4$ ) might be less effective in oxide reduction process since graphene growth could, in principle, be proceeding during the oxide strip. However, since good quality graphene has been realized with this protocol, the stripping of the oxide appears not be a constraint.

These results confirm a close relationship between the change in the Cu surface morphology under heat treatment and the nature of the graphene grains on the foil surface. The Cu surface morphology is modified by thermal treatment through the enlargement of grains and improved relative surface flatness. Here, grain growth is favored thermodynamically to decrease grain-boundary volume, which is less dense and much more defective than the crystalline bulk. The thermal energy provides the Cu mobility necessary to promote grain growth.

The simplistic view of CVD graphene growth that is often conveyed is that the catalytic substrate is perfectly flat and smooth. The organic feedstock is decomposed over this heated substrate, resulting in a shower of carbon atoms on the foil surface. The carbon adatoms move freely over the smooth and flat substrate until they reach a growing graphene grain front, where they bond onto the expanding grain, as

---

<sup>3</sup> Some contents in this chapter were published in Chemistry of Materials: Sarajlic, O. I.; Mani, R. G. "Mesoscale Scanning Electron and Tunneling Microscopy Study of the Surface Morphology of Thermally Annealed Copper Foils for Graphene Growth". Chem. Mater. 2013, 25, 1643–1648.



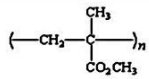
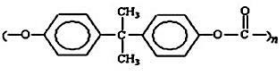
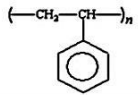
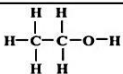
a result of an attractive interaction. Thus, the realization of large area Cu grains should improve surface flatness, adatom mobility, and C–C interactions which aids in the formation of graphene.

Although these results appear to be consistent with many aspects of this simplistic view, a puzzling aspect is that even within a single copper grain, which can be as large as several hundred micrometers, see Figure 4.12, we observe height variations that are very large compared to the diameter of the carbon atom, 0.22 nm. Certainly, the surface topography within a single grain appears not very flat, and deviations from flatness are not simple monatomic steps. In such a situation, adatom mobility and C–C interactions would presumably be reduced as adatoms are confronted with the height variations presented by the hilly topography. Yet, paradoxically, the growth of graphene film on such substrates seems not to be influenced by such topography.

## 6 POLYMER SUPPORT METHODS<sup>4</sup>

Before fabrication of the graphene-based electronic devices, graphene, with all its atoms being exposed to the molecular environment, is in need of careful choice of transfer mechanism and supporting substrate [10-13]. Graphene transfer onto a target substrate is a link between CVD growth of graphene on copper film and Hall bar device fabrication. This chapter concentrates on the effect of various thermoplastic materials used during the transfer of CVD-grown graphene. Before fabricating the monolayer graphene grown by CVD on copper, the foil with graphene was introduced to three different polymers, PMMA, PC, and PS, that act as mechanical transfer supports. The Cu substrate was etched with  $\text{FeCl}_3$  (0.34 M) solution, and the CVD graphene sheets with associated supporting materials were transferred onto  $\text{SiO}_2$  wafers. PMMA film was removed by immersing the graphene/polymer membrane on  $\text{SiO}_2$  in acetone bath, PC - in dichloromethane, and PS - in toluene for 20 hours. The cor-

Table 6.1 Molecular characteristics of thermoplastic polymers (PMMA, PC, and PS) and ethanol (ethyl alcohol). Molecular formula defines corresponding molecular structure. The geometry of PC and PS shows the existence of benzene rings that are attached to the carbon atom on the backbone of their chemical structures unlike the one of PMMA. Molecular characteristics of ethanol demonstrate the presence of hydroxyl group (-OH) that is able to dissolve many ionic and polar compounds and ethyl group ( $-\text{C}_2\text{H}_5$ ) that attracts non-polar substances.

Thermoplastic Polymer	Molecular Formula	Molecular Structure
Poly(methyl methacrylate) (PMMA)	$(\text{C}_5\text{O}_2\text{H}_8)_n$	
Polycarbonate (PC)	$(\text{C}_{16}\text{H}_{14}\text{O}_3)_n$	
Polystyrene (PS)	$(\text{C}_8\text{H}_8)_n$	
Solvent	Molecular Formula	Molecular Structure
Ethanol	$\text{C}_2\text{H}_6\text{O}$	

<sup>4</sup> The contents in this chapter are in review in Applied Physics Letters: Sarajlic, O. I.; Mani, R. G. "Various Polymer Support Methods of Transfer for CVD Graphene: Optical and Electronic Properties".

responding polymer solvents were exchanged twice during this process. Optical properties of transferred graphene films on  $\text{SiO}_2$  substrates were analyzed using SEM and Raman Spectroscopy.

The choice of alternative thermoplastic polymers to PMMA is mainly due to PC and PS having similar physical and chemical characteristics as those in PMMA. The polymer molecule structure for both PC and PS contains a benzene ring attached to the carbon atom on the backbone the molecular geometries which are shown in Table 6.1. In an attempt to decompose the residuals of the polymer from the graphene surface we introduce the carbon film to the ethanol treatment. Table 6.1 also shows the molecular structure of ethanol consists of an ethyl ( $-\text{C}_2\text{H}_5$ ) head and hydroxyl ( $-\text{OH}$ ) tail. Graphene transferred by the PMMA supporting method is indicated as GPMMA, graphene transferred with PMMA aid and then submerged to the ethanol treatment is denoted as EGPMMA. Similarly, the notations of GPC (GPS) and EGPC (EGPS) indicate graphene transferred by PC (PS) without ethanol and PC (PS) supported graphene after ethanol treatment, respectively.

## 6.1 Effect of Ethanol Treatment

Figure 6.1 shows SEM images of CVD graphene on  $\text{SiO}_2$  substrate and the effect of ethanol treatment on the cleanness of the graphene surface. Ethanol treatment in the case of graphene transferred via PMMA support partially cleaned the surface from the residuals of the polymer as Figure 6.1(b) suggests in comparison to the graphene membrane without ethanol bath, Figure 6.1(a). In addition to the visible changes to the surface, the electrical properties of graphene with PMMA support after ethanol treatment have also been enhanced as seen from Figure 6.3. Significant improvement to surface morphology of graphene on  $\text{SiO}_2$  is observed in the case of PC support before and after ethanol treatment when comparing Figures 6.1(c) – 6.1(d), which shows the rearrangement of polymer residue by ethanol. PS polymer was able to dissolve completely in corresponding solvent, toluene, suggesting that ethanol environment does not change the morphology of graphene film (Figures 6.1(e) – 6.1(f)). However, etha-

nol treatment positively affects the electrical properties of the graphene after its exposure to ethanol bath (see Figure 6.3).

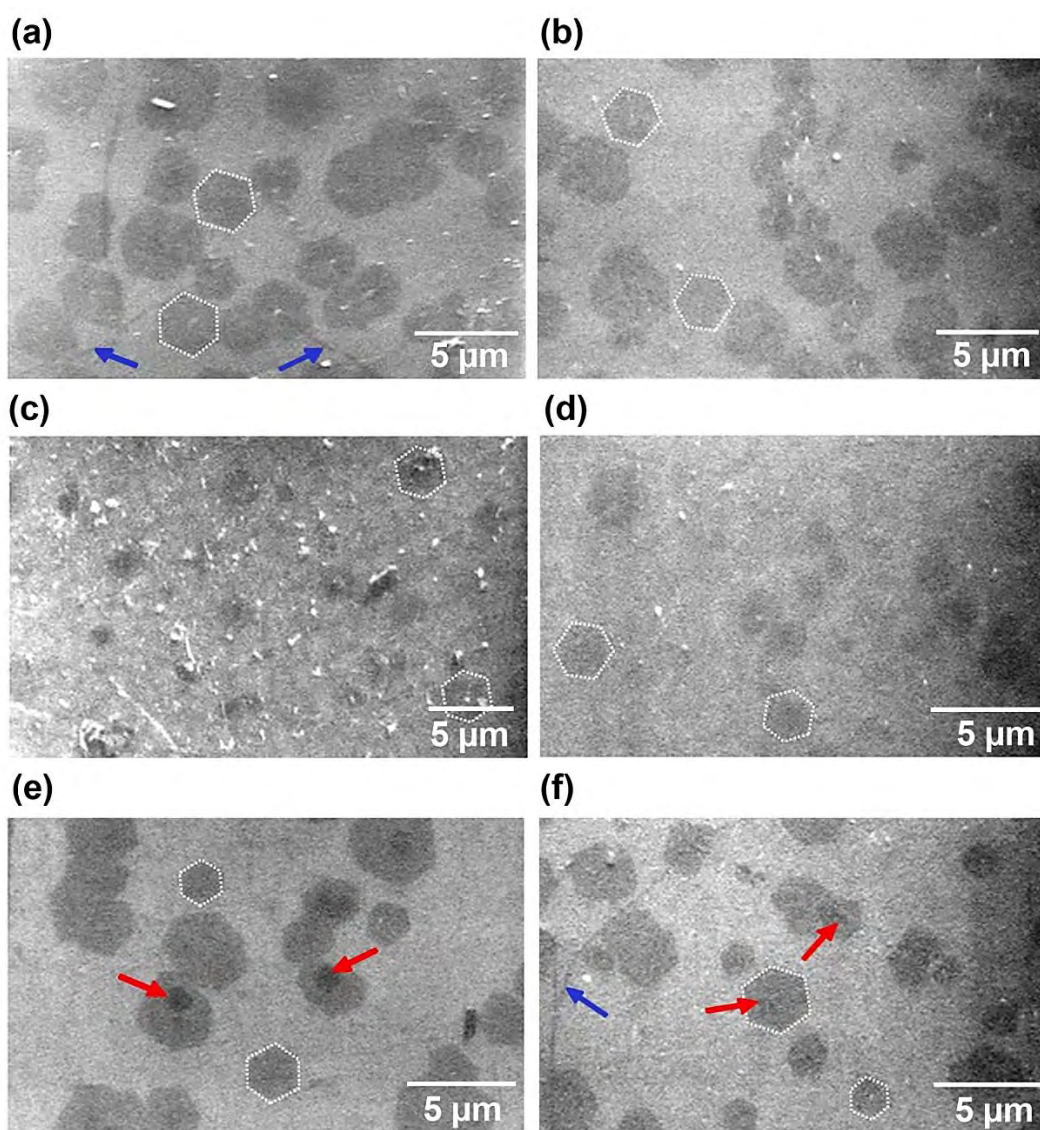


Figure 6.1 SEM images of CVD graphene on  $\text{SiO}_2$  substrate. (a) Graphene transferred via PMMA support showing visible wrinkles (blue errors) and graphene grains of about  $2\ \mu\text{m}$  each side of a hexagon. Scattered residuals of the polymer are clearly visible on the surface of the film. (b) Graphene transferred by PMMA, etched in acetone to remove PMMA, and then submerged to the ethanol bath. No noticeable wrinkles are observed, but the graphene grains of about  $2\ \mu\text{m}$  in length per side are present. (c) Graphene transferred by PC aid showing excess of polymer residuals on the surface. Graphene grains are still visible through the layer of unetched remnants of PC. (d) Graphene transferred by PC, etched in dichloromethane to remove PC, and then submerged to the ethanol bath. Ethanol treatment has evidently improved the cleanness of graphene film from polymer deposits. Graphene grains are still reproducible and clearly visible. (e) Graphene transferred by PS support showing visible adlayers (red errors) and graphene grains of about  $2\ \mu\text{m}$  each side of a hexagon. No visible residue of PS is observed. (f) Graphene transferred by PS, etched in toluene to remove thin layer of polymer support, and then submerged to the ethanol. Ethanol treatment does not have an observable effect on the appearance of the surface cleanness. Visible wrinkles (blue errors), adlayers (red errors), and graphene grains are observed on the surface of transferred graphene film.

## 6.2 Raman Characterizations of Ethanol Treated Graphene

Raman spectroscopy is utilized to analyze the behavior of G and 2D peaks as a function of thermoplastic polymer and ethanol treatment. Figure 6.2 shows the results of the Raman spectra of CVD graphene on SiO<sub>2</sub> substrate for all graphene transfer methods. The Raman D band at  $\sim 1350\text{ cm}^{-1}$ , which determines the defect density that is due to the zone-boundary phonons [66] within the material, has a relatively small intensity indicating a good quality of graphene. The Raman D band for graphene transferred by PMMA and PC is relatively small indicating a good quality of graphene. The intensity ratio of 2D to G bands ( $I_{2D}/I_G$ ) suggests that the surface of both samples is mostly covered by mono-layer graphene. The G band of EGPMMA is shifted by  $1.5\text{ cm}^{-1}$  to the right with respect to GPMMA G peak while 2D band of EGPMMA is shifted by  $\sim 3\text{ cm}^{-1}$  to the right with respect to the one of GPMMA. For the graphene transferred by PC aid, there observed a slight shift to the right of EGPC G peak of  $\sim 1\text{ cm}^{-1}$  comparing to the GPC G band while 2D peak of EGPC is being shifted to the right more drastically, by  $\sim 6\text{ cm}^{-1}$ . The intensity of the D band had been reduced in the case of graphene transferred by PS once treated with ethanol, suggesting that the ethanol bath potentially serves to provide polymer residual decomposition from the graphene surface. The G peak of EGPS experienced a  $3\text{ cm}^{-1}$  Raman shift to the right with respect to the GSP curve. The 2D EGPS band is shifted to the right by  $4\text{ cm}^{-1}$  with respect to the GPS 2D band. The following observations suggest that the ethanol treatment has a slight effect on the Raman spectrography of the graphene quality.

Raman spectrograph data of the G and 2D band position shift show consistent blue-shift of the curves for the graphene films that were treated by ethanol, regardless of the polymer support used during the transfer. This minor blue-shift is less likely to be caused by the compressive stress on graphene film by the SiO<sub>2</sub> substrate [69] because the samples did not experience any thermal treatment that would be a source of stress. The narrowing of the G and 2D bandwidth was observed in case of gra-

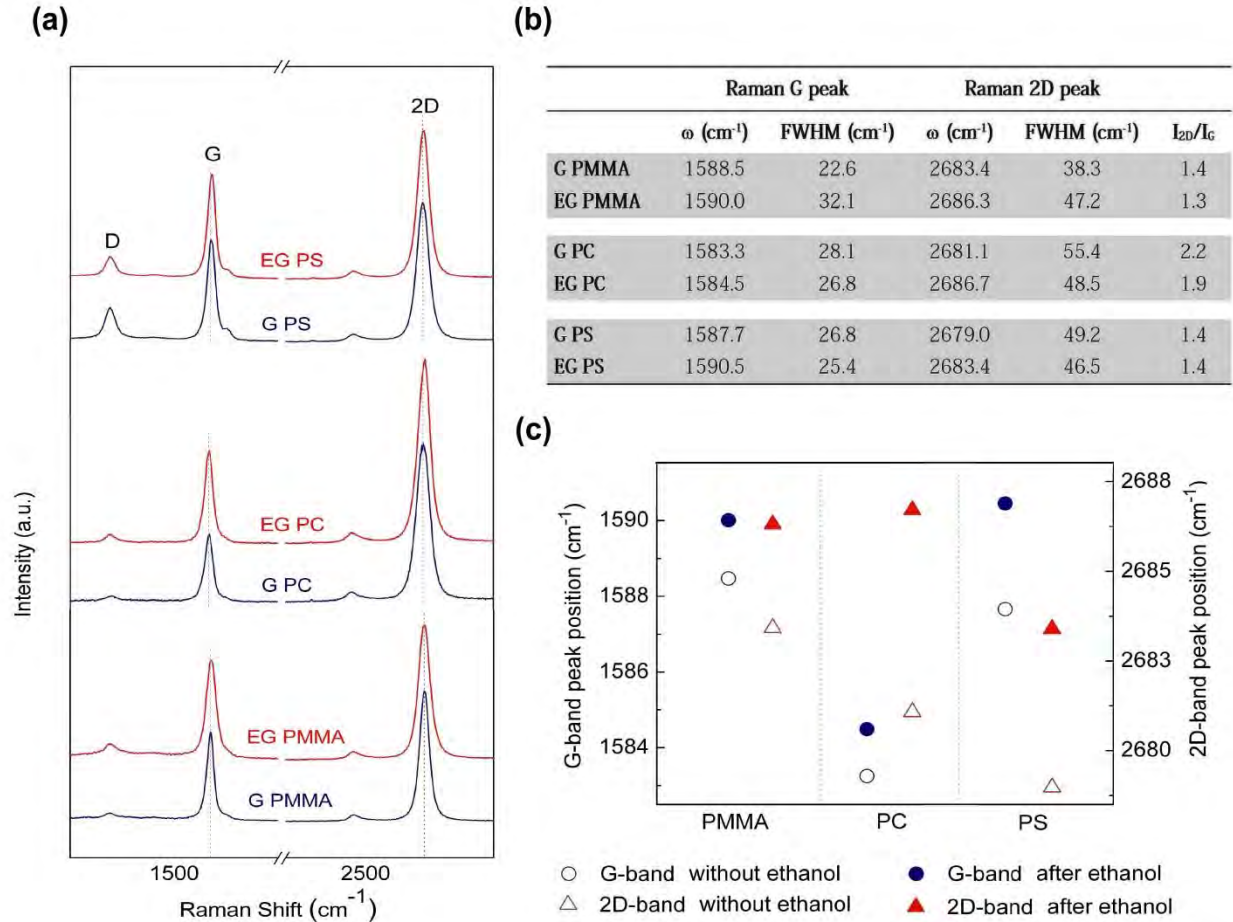


Figure 6.2 (a) Raman spectra of CVD graphene on  $\text{SiO}_2$  substrate (using 532 nm wavelength laser) transferred by PMMA (bottom blue curve), PMMA then ethanol treatment (bottom red curve), PC (middle blue curve), PC then ethanol treatment (middle red curve), PS (top blue curve), and PS then ethanol treatment (top red curve). Raman spectroscopy shows consistent blue-shift of the curves of graphene that were treated by ethanol, regardless of the polymer support used during the transfer. (b) Raman characteristics of CVD graphene on  $\text{SiO}_2$  substrate transferred by PMMA, PC, and PC polymer support materials in addition to those exposed to the ethanol bath, indicated as EG PMMA, EG PC, and EG PS. (c) G-band and 2D-band peak positions as a function of transferred polymer that are extracted from corresponding Raman spectra (a). Both peaks trend to exhibit a blue-shift after the graphene films were exposed to ethanol.

phene transferred by PC and PS polymers after the ethanol treatment, suggesting the doping effect which owes to the Pauli Exclusion Principle for electrons and holes where the phonon cannot decay into electron-hole pairs because of the absence of the resonant process[68]. In addition, the ethanol treated samples show that graphene transferred by PMMA and PC polymer experience a reduction in  $I_{2D}/I_G$  ratio which also signifies the doping effect [68]. The observed G and 2D band blue-shifts on average by  $\sim 2$

$\text{cm}^{-1}$  for G band and by  $\sim 4 \text{ cm}^{-1}$  for 2D band suggest that the graphene samples are more p-doped after the ethanol treatment.

The table in Figure 6.2(b) shows the Raman characteristics of CVD graphene on  $\text{SiO}_2$  substrate transferred by PMMA, PC, and PC polymer support materials in addition to those exposed to the ethanol. The intensity ratios of 2D to G bands  $I_{2D}/I_G$  vary from 1.3 to 2.2 in both cases, graphene without ethanol treatment and with ethanol treatment, respectively. The values of  $I_{2D}/I_G$  ratios indicate that the graphene is mostly a single layer with an exception of adlayers, as seen from Figure 6.1, which would trigger the elevation of number of layer in graphene and reduction of corresponding  $I_{2D}/I_G$  ratios.

Raman data are measured to compare the behavior of graphene before and after the ethanol treatment. Raman characteristics along with the Raman analysis table on Figure 6.2(b) confirm that the G and 2D peaks tend to exhibit a blue-shift after the graphene films were exposed to the ethanol treatment. Therefore, the change in the Raman spectra of ethanol treated graphene samples gives rise to a shift to higher frequency in both G and 2D bands due to ethanol ability to dissolve and/or rearrange the residuals of the polymer from the graphene surface [54]. In addition, ethanol treatment has a tendency to dope graphene toward p-type material.

### 6.3 Electrical Measurements as a Function of Polymer Support

In an attempt to improve the electrical properties of graphene, the Hall bar devices that were exposed to PMMA, PC, and PS support polymers were treated in ethanol. Plastics are commonly absorbent to organic chemicals the effects of which include dissolution and/or recrystallization [54]. Thus, ethanol treatment may potentially rearrange the polymer residue where the hydroxyl functional group is able to dissolve many ionic and polar compounds while the ethyl group attracts non-polar substances [55].

Four-terminal electrical measurements were carried out at room temperature. Charge carrier mobility is measured as a function of the thermoplastic polymer support before and after the ethanol

treatment as shown on Figure 6.3. We measured nine devices before and nine devices after the exposure to the ethanol treatment. The samples fabricated using PMMA transfer support had mobility of  $1148 \pm 518 \text{ cm}^2/(\text{V}\cdot\text{s})$  before ethanol treatment, and  $1338 \pm 1134 \text{ cm}^2/(\text{V}\cdot\text{s})$  after ethanol bath. Graphene devices transferred by PC had mobility of  $1382 \pm 291 \text{ cm}^2/(\text{V}\cdot\text{s})$  before ethanol treatment, and  $1594 \pm 206 \text{ cm}^2/(\text{V}\cdot\text{s})$  after ethanol solvent. Devices transferred by PS aid had mobility of  $1779 \pm 992 \text{ cm}^2/(\text{V}\cdot\text{s})$  before ethanol treatment, and  $2283 \pm 1366 \text{ cm}^2/(\text{V}\cdot\text{s})$  after ethanol. All devices, regardless of the polymer support mechanism, had on average of about 21% increase in charge carrier mobility at room temperature in air when allowing  $\text{SiO}_2/\text{graphene}$  structure to be exposed to the ethanol treatment. The reason for the evident enhancement of the electrical properties of CVD-grown graphene devices after the ethanol treatment could be due to ethanol acting as an additional solvent due to the fact that plastics, in general, are permeable to organic compounds which in turn considerably removes the residuals of the polymer. Based on SEM characterizations, ethanol treated graphene surface improved substantially by having minimal remnants of polymer residue.

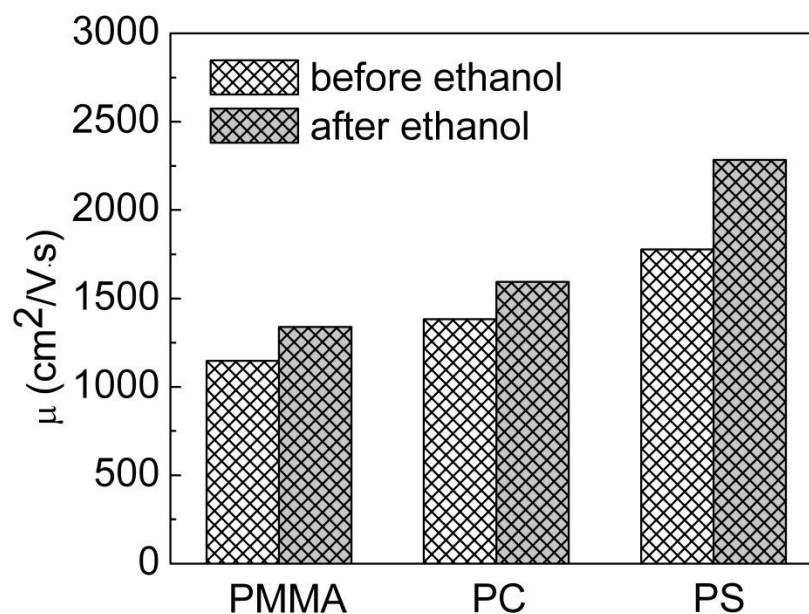


Figure 6.3 Mobility of CVD graphene samples as a function of transfer polymer. The bar chart compares the ethanol treatment impact on the electrical characteristics of transferred graphene (G) by PMMA, PC, and PS. Ethanol



treated graphene (EG) samples have a tendency to exhibit higher mobility regardless of the polymer aid that is used for transfer.

The results of the study demonstrated the difference of the polymer choice during the graphene transfer and the importance of the ethanol treatment on the surface characterization and electrical properties of graphene. Significant improvement to surface morphology of graphene on SiO<sub>2</sub> is observed after the ethanol treatment. Besides the change in cleanness of the graphene surface, all devices that had been treated with ethanol, regardless of choice of polymer aid, showed significant improvement in carrier mobility. Raman characterization of the graphene samples showed noticeable blue-shifts in G and 2D band which results suggest that the graphene samples are more p-doped after the ethanol treatment.

#### **6.4 Graphene Surface Tears**

Even though, there is a considerable improvement to the mobility of the graphene after the film has been subjected to the ethanol bath when comparing electronic properties of graphene transferred by both PC and PS, graphene transferred by PMMA results in less tears of the graphene membrane as seen on Figure 6.4(a). Figure 5.4(b) shows PC aid of graphene transfer which results in larger and less frequent tears than those on the graphene transferred by PS (~ 40 slits per ~ 0.5 mm<sup>2</sup> sample area). Graphene transferred by PC exhibits approximately 25% less tears in addition to the absence of fractures comparing to the film transferred with PS aid.

PS supported transfer leads to small but frequent tears (~ 53 slits per ~ 0.5 mm<sup>2</sup> sample area) as well as film laceration as there are few fractures observed on the surface (Figure 6.4(c)). Polymers made from ethylene such as PMMA are much more elastic than the brittle polymers synthesized from styrene such as PS. PC is still inelastic in comparison to the PMMA molecule. That is why the tears are more likely to be induced on the surface of graphene during transfer due to the flexibility of corresponding thermoplastic polymer as discussed earlier with reference to Table 6.1.

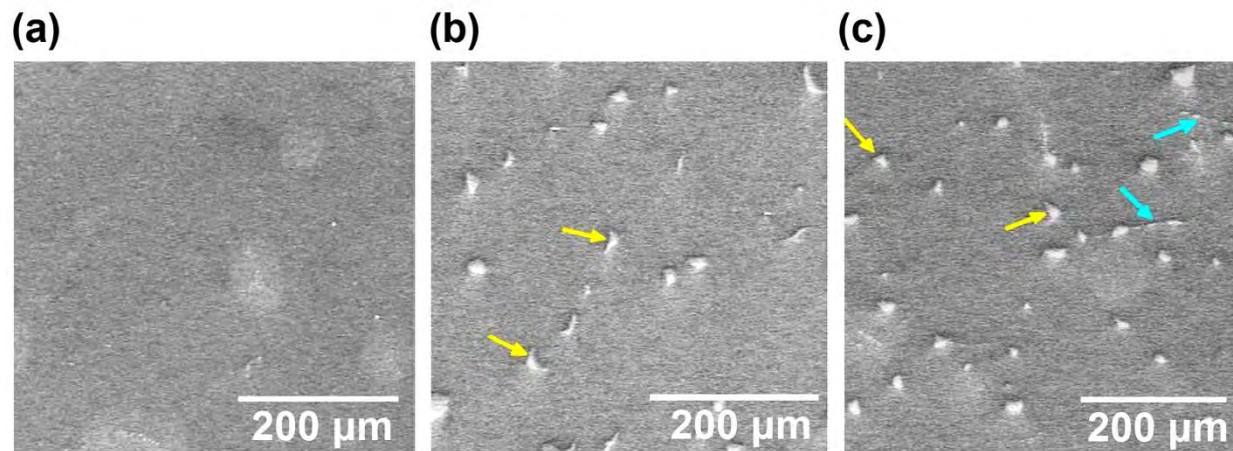


Figure 6.4 SEM images of CVD graphene on SiO<sub>2</sub> substrate that have been treated with ethanol. (a) Large scale graphene film transferred via PMMA support showing no visible breaks or tears of graphene membrane. (b) Graphene transferred by PC aid showing larger area tears (yellow errors) and no visible fractures or laceration of graphene film. (c) Graphene transferred by PS support showing visible small but frequent tears (yellow errors) along with partial laceration (turquoise errors) of the membrane going across the chain of slits.

## 7 SUMMARY AND FUTURE WORK

The surface topography of bare- and etched- thermally treated copper foils have been examined by optical microscopy, SEM, and STM. Cu foils were subjected to chemical pretreatment and pre-annealing procedures with the intention of improving the quality of Cu film and providing better conditions for graphene growth. The results showed that etching copper foils scars the surface and leaves behind etch quarries and residue. The protocol that included pre-annealing of foils followed by the growth process was expected to improve the quality of the foil surface, sequentially resulting in a better quality of graphene. However, this procedure produced a crust layer on the foil that sometimes peeled off along with graphene. The STM study indicated that the heat treated Cu surface includes large height variations on the micrometer length scale. Yet, a layer of graphene on top of the Cu surface reduced its apparent surface roughness. Optical micrograph of CVD graphene transferred onto a  $\text{SiO}_2$  wafer displays the imprinted surface texture of the Cu grain boundaries on the subsequently grown graphene layer. This observation supports the notion that carbon atoms bind more readily at the Cu grain boundary during the CVD growth.

The results of Chapter 6 demonstrated the difference in PMMA, PC, and PS thermoplastic polymers during the graphene transfer and the importance of the ethanol treatment on the surface characterization and electrical properties of graphene. Visible improvement to surface morphology of graphene on  $\text{SiO}_2$  is observed after the ethanol treatment. Besides the change in cleanness of the graphene surface, all devices that had been treated with ethanol, regardless of choice of polymer aid, showed noticeable improvement in carrier mobility. Raman characterization of the graphene samples showed evident blue-shifts in the G and 2D bands which suggest that the graphene samples are more p-doped after the ethanol treatment. Even though, there is a distinct improvement to the electrical properties of graphene after the film has been subjected to the ethanol treatment. Graphene transferred by both PC and

PS showed visible tears along with partial laceration of the graphene membrane, unlike graphene transferred by PMMA, which results in less tears of the carbon film.

The future work will consist of the extension of graphene study. Magnetoresistance (MR) measurements on CVD graphene will be performed at room temperature down to liquid helium temperatures. Measurement results will be analyzed as a function of temperature variations, and the expected weak localization (WL) features will provide the information about the quality of the sample, as WL is caused by the inter-valley scattering due to the presence of atomically sharp disorders which in turn favors the appearance of WL at zero magnetic field. Given the existence of such structure, the dependence of WL on magnetic field will be fitted by the McCann theory on WL [70], and extracted characteristics length scales: phase coherence length,  $L_\phi$ , inter-valley scattering length,  $L_i$ , and intra-valley scattering length,  $L_*$ , will be analyzed as a function of temperature and carrier density. We will also study a dependence of various carrier temperatures as a function of a given current for devices of various carrier density and mobility.

## REFERENCES

- [1] Novoselov, K. S.; Geim, A. K.; Morozov, S. V.; Jiang, D.; Zhang, Y.; Dubonos, S. V.; Grigorieva, I. V.; Firsov, A. A., *Science* 2004, 306, 666.
- [2] Zhang, Y.; Tan, Y. W.; Stormer, H. L.; Kim, P., *Nature* 2005, 438, 201.
- [3] Novoselov, K. S.; McCann, E.; Morozov, S. V.; Fal'ko, V. I.; Katsnelson, M. I.; Zeitler, U.; Jiang, D.; Schedin, F.; Geim, A. K. *Nat. Phys.* 2006, 2, 177.
- [4] Geim, A. K. *Science* 2009, 324 (5934), 1530–1534.
- [5] Li, X.; Magnuson, C. W.; Venugopal, A.; Tromp, R. M.; Hannon, J. B.; Vogel, E. M.; Colombo, L.; Ruoff, R. S. *J. Am. Chem. Soc.* 2011, 133, 2816–2819.
- [6] Chen, S.; Cai, W.; Piner, R. D.; Suk, J. W.; Wu, Y.; Ren, Y.; Kang, J.; Ruoff, R. S. *Nano Lett.* 2011, 11, 3519–3525.
- [7] Li, X. S.; Cai, W. W.; An, J. H.; Kim, S.; Nah, J.; Yang, D. X.; Piner, R. D.; Velamakanni, A.; Jung, I.; Tutuc, E.; et al. *Science* 2009, 324, 1312–1314.
- [8] Li, X.; Cai, W.; Colombo, L.; Ruoff, R. S. *Nano Lett.* 2009, 9, 4268–4272.
- [9] Sarajlic, O. I.; Mani, R. G. *Chem. Mater.* 2013, 25, 1643–1648.
- [10] Chen, X. D.; Liu, Z. B.; Zheng, C. Y.; Xing, F.; Yan, X. Q.; Chen, Y.; Tian, J. G. *Carbon* 2013, 56, 271.
- [11] Reina, A.; Son, H.; Jiao, L.; Fan, B.; Dresselhaus, M. S.; Liu, Z. F.; Kong, J. J. *Phys. Chem.* 2008, 112, 17741.
- [12] Liang, X.; Sperling, B. A.; Calizo, I.; Cheng, G.; Hacker, C. A.; Zhang, Q.; Obeng, Y.; Yan, K.; et. al. *ACS Nano* 2011, 5, 9144.
- [13] Suk, J. W.; Kitt, A.; Magnuson, C. W.; Hao, Y.; Ahmed, S.; An, J.; Swan, A. K.; Goldberg, B. B.; Ruoff, R. S. *ACS Nano* 2011, 5(9), 6916-6924.
- [14] Scarselli, M.; Castrucci, P.; De Crescenzi, M. J. *Phys.: Condens. Matter* 2012, 24, 313202.
- [15] Geim, A. K.; Novoselov, K. S. *Nat. Mater.* 2007, 6, 183–191.

- [16] De Heer, W. A.; Berger, C.; Wu, X.; Sprinkle, M.; Hu, Y.; Ruan, M.; Stroschio, J. A.; First, P. N.; Haddon, R.; Piot, B.; et al. *J. Phys. D: Appl. Phys.* 2010, 43, 374007.
- [17] Guermoune, A.; Chari, T.; Popescu, F.; Sabri, S. S.; Guillemette, J.; Skulason, H. S.; Szkopek, T.; Siaj, M. *Carbon* 2011, 49, 4204–4210.
- [18] Virojanadara, C.; Syväjärvi, M.; Yakimova, R.; Johansson, L. I.; Zakharov, A. A.; Balasubramanian, T. *Phys. Rev. B* 2008, 78, 245403.
- [19] Berger, C.; Song, Z.; Li, X.; Wu, X.; Brown, N.; Naud, C.; Mayou, D.; Li, T.; Hass, J.; Marchenko, A. N.; et al. *Science* 2006, 312, 1991–1996.
- [20] Emtsev, K. V.; Bostwick, A.; Horn, K.; Jobst, J.; Kellogg, G. L.; Ley, L.; et al. *Nature Materials* 2009, 8, 203–207.
- [21] Luo, Z.; Lu, Y.; Singer, D. W.; Berck, M. E.; Somers, L. A.; Goldsmith, B. R.; Johnson, A. T. C. *Chem. Mater.* 2011, 23, 1441–1447.
- [22] Chen, S.; Brown, L.; Levendorf, M.; Cai, W.; Ju, S. Y.; Edgeworth, J.; Li, X.; Magnuson, C. W.; Velamakanni, A.; Piner, R. D.; et al. *ACS Nano* 2011, 5, 1321–1327.
- [23] Cho, J.; Gao, L.; Tian, J.; Cao, H.; Wu, W.; Yu, O.; Yitamben, E. N.; Fisher, B.; Guest, J. R.; Chen, Y. P.; et al. *ACS Nano* 2011, 5, 3607–3613.
- [24] Li, X. S.; Cai, W. W.; Jung, I. H.; An, J. H.; Yang, D. X.; Velamakanni, A.; Piner, R.; Colombo, L.; Ruoff, R. S. *ECS Trans.* 2009, 19, 41–52.
- [25] Giorgi, R.; Lisi, N.; Dikonimos, T.; Falconieri, M.; Gagliardi, S.; Salernitano, E.; Morales, P.; Pilloni, L. *EAI* 2011, 68–74.
- [26] Robinson, Z. R.; Tyagi, P.; Murray, T. M.; Ventrice, C. A., Jr.; Chen, C.; Munson, A.; Magnuson, C. W.; Ruoff, R. F. *J. Vac. Sci. Technol. A* 2012, 30 (1), 011401/1–011401/7.
- [27] Chen, H.; Zhu, W.; Zhang, Z. *Phys. Rev. Lett.* 2010, 104, 186101.

- [28] Mayorov, A. S.; Gorbachev, R. V.; Morozov, S. V.; Britnell, L.; Jalil, R.; Ponomarenko, L. A.; Blake, P.; Novoselov, K. S.; Watanabe, K.; Taniguchi, T. et al. *Nano Lett.* 2011, 11, 2396-2399.
- [29] Li, X.; Magnuson, C. W.; Venugopal, A.; An, J.; Suk, J. W.; Han, B.; Borysiak, M.; Cai, W.; Velamakanni, A.; Zhu, Y. *Nano Lett.* 2010, 10, 4328-4334.
- [30] S. Bae, S.; H. Kim, H.; Y. B. Lee, Y. B.; X. F. Xu, X. F.; J. S. Park, J. S.; Y. Zheng, Y.; J. Balakrishnan, J.; T. Lei, T.; Kim, H. R.; Song, Y. I.; et al. *Nat. Nanotechnol.* 2010, 5, 574.
- [31] Yu, Q.; Jauregui, L. A.; Wu, W.; Colby, R.; Tian, J. F.; Su, Z. H.; Cao, H. L.; Liu, Z. H.; Pandey, D.; Wei, D. G.; et al., *Nature Mater.* 2011, 10, 44.
- [32] Yazyev, O. V.; Pasquarello, A. *Phys. Rev. Lett.* 2008, 100, 156102/1-156102/4.
- [33] Yu, Q.; Jauregui, L. A.; Wu, W.; Colby, R.; Tian, J.; Su, Z.; Cao, H.; Liu, Z.; Pandey, D.; Wei, D. *Nat. Mater.* 2011, 10, 443-449.
- [34] Bae, S.; Kim, H.; Lee, Y.; Xu, X.; Park, J. S.; Zheng, Y.; Balakrishnan, J.; Lei, T.; Kim, H. R.; Song, Y. I.; et al. *Nat. Nanotechnol.* 2010, 5, 574-578.
- [35] Cao, H.; Yu, O.; Jauregui, L. A.; Tian, J.; Wu, W.; Liu, Z.; Jalilian, R.; Benjamin, D. K.; Jiang, Z.; Bao, J.; et al. *Appl. Phys. Lett.* 2010, 96, 122106.
- [36] Zhao, L.; Rim, K. T.; Zhou, H.; He, R.; Heinz, T. F.; Pinczuk, A.; Flynn, G. W.; Pasupathy, A. N. *arXiv:1008.3542v1*, 2010.
- [37] Zhang, B.; Lee, W. H.; Piner, R.; Kholmanov, I.; Wu, Y.; Li, H.; Ji, H.; Ruoff, R. S. *ACS Nano* 2012, 6 (3), 2471-2476.
- [38] Han, Z.; Kimouche, A.; Allain, A.; Arjmandi-Tash, H.; Reserbat-Plantey, A.; Pairis, S.; Reita, V.; Bendiab, N.; Coraux, J.; Bouchiat, V. *arXiv: 1205.1337*, 2012.
- [39] Yazyev, O. V.; Louie, S. G. *Nat. Mater.* 2010, 9, 806-809.
- [40] Huang, P. Y.; Ruiz-Vargas, C. S.; van der Zande, A. M.; Whitney, W. S.; Garg, S.; Alden, J. S.; Hustedt, C. J.; Zhu, Y.; Park, J.; McEuen, P. L.; et al. *Nature* 2011, 469, 389-392.

- [41] Kim, K.; Lee, Z.; Regan, W.; Kisielowski, C.; Crommie, M. F.; Zettl, A. *ACS Nano* 2011, 5 (3), 2142–2146.
- [42] Mattevi, C.; Kim, H.; Chhowalla, M. J. *Mater. Chem.* 2010, 21, 3324–3334.
- [43] Chen, Y. P.; Yu, Q. K. *Nat. Nanotechnol.* 2010, 5, 559–560.
- [44] Lin, Y. C.; Lu, C. C.; Yeh, C. H.; Jin, C.; Suenaga, K.; Chin, P. W. *Nano Lett.* 2012, 12, 414.
- [45] Booth, T. J.; Blake, P.; Nair, R. R.; Jiang, D.; Hill, E. W.; Bangert, U.; Bleloch, A.; Gass, M.; Novoselov, K. S.; Katsnelson, M. I.; Geim, A. K. *Nano Lett.* 2008, 8, 2442.
- [46] Lin, Y. C.; Jin, C.; Lee, J. C.; Jen, S. F.; Suenaga, K.; Chiu, P. W. *ACS Nano* 2011, 5, 2362.
- [47] Suk, J. W.; Lee, W. H.; Lee, J.; Chou, H.; Piner, R. D.; Hao, Y.; Akinwande, D.; Ruoff, R. S. *Nano Lett.* 2013, 0.1021/nl304420b.
- [48] Ryu, S.; Liu, L.; Berciaud, S.; Yu, Y. J.; Liu, H.; Kim, P.; Plyn, G. W.; Brus, L. E. *Nano Lett.* 2010, 10, 4944.
- [49] Stuart, B. H. *Polymer Analysis*, Wiley, 2002, 4.
- [50] Ishigami, M.; Chen, J. H.; Cullen, W. G.; Fuhrer, M. S.; Williams, E. D. *Nano Letters* 2007, 7(6), 1643-1648.
- [51] Schedin, F.; Geim, A. K.; Morozov, S. V.; Hill, E. W.; Blake, P.; Katsnelson, M. I.; Novoselov, K. S. *Nat. Mater.* 2007, 6, 652.
- [52] Chen, J. H.; Jang, C.; Adam, S.; Fuhrer, M. S.; Williams, E. D.; Ishigami, M. *Nature Physics* 2008, 4(5), 377–381.
- [53] Margolis, J. M., *Engineering Thermoplastics: Properties and Applications*, Marcel Dekker, Inc., 1985, 1.
- [54] American Society of Metals. *Characterization and Failure Analysis of Plastics*, ASM International, 2003, 323.
- [55] Mehta, B.; Mehta, M. *Organic Chemistry*, Prentice-Hall of India Pvt.Ltd, 1, 2005.



- [56] Nakada, K.; Fujita, M.; Dresselhaus, G.; Dresselhaus, M. S. *Phys. Rev. B* 1996, 54, 17954-61.
- [57] Niimi, Y.; Matsui, T.; Kambara, H.; Tagami, K.; Tsukada, M.; Fukuyama, H. *Phys. Rev. B*. 2006, 73, 85421-851.
- [58] Neto, A. H. C.; Guinea, F.; Peres, N. M. R.; Novoselov, K. S.; Geim, A. K. *Rev. Mod. Phys.* 2009, 81, 109–162.
- [59] Falkovsky, L. A. *J. Phys.* 2008, 129(1), 012004.
- [60] Semenoff, G. W. *Phys. Rev. Lett.* 1984, 53, 2449–2452.
- [61] Avouris, P.; Chen, Z.; Perebeinos, V. *Nature Nanotechnology* 2007, 2(10), 605–615.
- [62] Soldano, C.; Manmood, A.; Dujardin, E. *Carbon* 2010, 48, 2127.
- [63] Jie Song, J.; Kam, F. Y.; Png, R. Q.; Seah, W. L.; Zhuo, J. M.; Lim, G. K.; Ho, P. K. H.; Chua, L.L. *Nature Nanotechnology* 2013, 8, 356–362.
- [64] Wu, W.; Yu, Q.; Peng, P.; Liu, Z.; Bao, J.; Pei, S. S. *Nanotechnology* 2012, 23, 035603.
- [65] Bojan, M.; Schiopu, P.; Garoi, I.; Iordache, J.; Apostol, D. *U.P.B. Sci. Bull. 2012, Series A, Vol. 74, Issue 2.*
- [66] Ferrari, A. C.; Meyer, J. C.; Scardaci, V.; Casiraghi, C.; Lazzeri, M.; Mauri, F.; Piscanec, S.; Jiang, D.; Novoselov, K. S.; Roth, S.; et al. *Phys. Rev. Lett.* 2006, 97 (18), 187401/1–187401/4.
- [67] Ni, Z.; Wang, Y.; Yu, T.; Shen. *Nano Res.* 2008, 1, 273–291.
- [68] Ni, Z. H.; Wang, H. M.; Luo, Z. Q. Wang, Y. Y.; Yu, T.; Wu, Y. H.; Shen, Z. X. *J. Raman Spectrosc.* 2010, 41, 479.
- [69] Ni, Z. H.; Wang, H. M.; Ma, Y.; Kasim, J.; Wu, Y. H.; Shen, Z. X. *ACS Nano* 2008, 2, 1033.
- [70] McCann, E.; Kchedzhi, K.; Fal'ko, V. I.; Suzuura, H.; Ando, T.; Altshuler, B. L. *PRL* 2006, 97, 146805.
- [71] Stoller, M. D.; Park, S.; Zhu, Y.; An, J.; Ruoff, R. S. *Nano Lett.* 2008, 8(10), 3498.

## APPENDICES

### Appendix A: List of Abbreviations

AFM	–	Atomic Force Microscope
BF	–	Bare foil
CVD	–	Chemical Vapor Deposition
EF	–	Etched foil
EG	–	Ethanol treated graphene
G	–	Graphene transferred by PMMA, PC, and PS
$L_\varphi$	–	Phase coherence length
$L_i$	–	Inter-valley scattering length
$L_*$	–	Intra-valley scattering length
MR	–	Magnetoresistance
OM	–	Optical Microscope
PC	–	Polycarbonate
PDMS	–	Polydimethylsiloxane
PMMA	–	Poly(methyl methacrylate)
PS	–	Polystyrene
$R_a$	–	Average Roughness
SEM	–	Scanning Electron Microscope
STM	–	Scanning Tunneling Microscope
UHV	–	Ultra High Vacuum
WL	–	Weak Localization

## Appendix B: Methods

### ***Appendix B.1: Graphene Growth in Chapter 4***

CVD synthesis of graphene samples were performed on 25  $\mu\text{m}$  thick copper foil using a horizontal 1 inch quartz tube furnace system. All foil specimens came from the same roll. The method involved the flow of methane and hydrogen/nitrogen gases. Under vacuum conditions with the base pressure of 36 mTorr, the furnace is heated to 1025  $^{\circ}\text{C}$  with 10 sccm flow of  $\text{H}_2\text{N}_2$  reaching 200 mTorr  $\text{H}_2\text{N}_2$  pressure. Once the temperature reached 1025  $^{\circ}\text{C}$ , the flow of  $\text{CH}_4$  is introduced to the system. Both  $\text{CH}_4$  with 40 sccm and  $\text{H}_2\text{N}_2$  with 10 sccm are flowing during the growth process at 1025  $^{\circ}\text{C}$  for 30 min ( $P \sim 500$  mTorr). During the CVD growth, the furnace with the Cu foil required a period of 30 min to reach the operating temperature of 1025  $^{\circ}\text{C}$ . During this period, there was a steady flow of  $\text{H}_2\text{N}_2$  in the growth chamber. After heat treatment, the specimens were cooled to room temperature over a period of two hours.

### ***Appendix B.2: Graphene Growth in Chapter 6***

Commercially available 25  $\mu\text{m}$  Cu foils were used. All foil specimens came from the same roll. The heat treatment of the foils was carried out in a mechanically pumped CVD system consisting of 1" furnace with 1" o.d. quartz tube. The CVD system was supplied with high purity  $\text{H}_2\text{:N}_2$  [10%:90%] and  $\text{CH}_4$ . The growth process took 30 minutes at 1000  $^{\circ}\text{C}$  under  $\text{H}_2\text{N}_2\text{:CH}_4$  [10 sccm : 65 sccm] with  $P=375$  mTorr. Before CVD growth, the furnace with the Cu foil required a period of 30 minutes to reach the operating temperature of 1000  $^{\circ}\text{C}$ . During this period, there was a steady flow of  $\text{H}_2\text{N}_2$  in the growth chamber with  $P=216$  mTorr. After the growth has been completed, the specimens were cooled to room temperature at a cooling rate of  $\sim 8$   $^{\circ}\text{C}/\text{min}$ .

### ***Appendix B.3: Graphene Transfer in Chapter 4***

PMMA transfer method was utilized as a supporting mechanical substrate. PMMA solution was spin-coated onto the graphene/Cu substrate with 500 rpm for 3 seconds following by 4500 rpm for 60 seconds and then back to 500 rpm for 5 seconds. The copper film was chemical etched with  $\text{Fe}(\text{NO}_3)_3$  (1M) solution, followed by thorough rinsing with deionized water. Silicon dioxide served as a substrate of choice for the graphene/polymer system. The graphene/polymer support membrane was allowed to air-dry for the period of 24 hours on the  $\text{SiO}_2$  substrate. Then, the PMMA was soaked in acetone overnight and dried with nitrogen gas.

### ***Appendix B.4: Graphene Transfer in Chapter 6***

Poly(methyl methacrylate) (PMMA), polycarbonate (PC), and polystyrene (PS) transfer methods were utilized as a supporting mechanical substrates. These polymer glass solutions were spin-coated onto the graphene/Cu substrate with 500 rpm for 3 seconds following by 4500 rpm for 60 seconds and then back to 500 rpm for 5 seconds. The copper film was chemically etched with  $\text{FeCl}_3$  (0.34 M) solution, followed by thorough rinsing with deionized water. The  $\text{SiO}_2$  served as a substrate of choice for graphene/polymer membrane. The membrane was allowed to air-dry for the period of 24 hours on the  $\text{SiO}_2$  substrate. Then, the PMMA was soaked in acetone, PC - in dichloromethane, and PS - in toluene baths for 20 hours and dried with nitrogen gas. Chemical treatment with ethanol for each graphene sample on  $\text{SiO}_2$  substrate was performed for 20 hours.

### ***Appendix B.5: Sample Fabrication Technique in Chapter 6***

Graphene sheet deposition onto  $\text{SiO}_2$  substrate was performed using the support of the proposed thermoplastic polymers after the etching process of Cu foil in  $\text{FeCl}_3$  solution has been completed. Fabrication of Hall bars was done by the photo-lithography, using the oxygen plasma

treatment for graphene Hall bar development. Ethanol treated devices were submerged in ethanol bath for 20 hours prior to the measurement performance.

***Appendix B.6: Optical Technology Classifications in Chapter 4***

Optical images were taken with Metallographic microscope, XJP-H100 series. SEM characterization was performed using Cambridge Instruments, Stereoscan 360 with a substrate at room temperature with chamber vacuum at  $8.5 \times 10^{-6}$  Torr and column vacuum at  $1.1 \times 10^{-7}$  Torr. STM classification was done using Ultra High Vacuum (UHV) RHK chamber with a substrate at room temperature with chamber vacuum at  $1 \times 10^{-7}$  Torr.

***Appendix B.7: Optical Technology Classifications in Chapter 6***

SEM characterization was performed using Cambridge Instruments, Stereoscan 360 with a substrate at room temperature with chamber vacuum at  $8.5 \times 10^{-6}$  Torr and column vacuum at  $1.1 \times 10^{-7}$  Torr. Raman spectra were attained on CVD graphene on  $\text{SiO}_2$  substrate transferred by various polymer glass support methods. The measurements are performed at room temperature with a LabRAM HR spectrometer at 532 nm wavelength laser excitation, with scan area of 1  $\mu\text{m}$  in diameter. A 50 $\times$  objective is used.